THE JOURNAL OF BIOLOGICAL CHEMISTRY VOL. 288, NO. 39, pp. 28034–28048, September 27, 2013

Assembly of Functional Ribonucleoprotein Complexes by AU-rich Element RNA-binding Protein 1 (AUF1) Requires Base-dependent and -independent RNA Contacts*

Received for publication, May 28, 2013, and in revised form, August 2, 2013 Published, JBC Papers in Press, August 12, 2013, DOI 10.1074/jbc.M113.489559

Beth E. Zucconi[1] **and Gerald M. Wilson**[2]

From the Department of Biochemistry and Molecular Biology and Marlene and Stewart Greenebaum Cancer Center, University of Maryland School of Medicine, Baltimore, Maryland 21201

Background: AUF1 post-transcriptionally regulates mRNA targets.
Results: Short AU-rich sequences nucleate AUF1 ribonucleoproteins but require non-ionic contacts with flanking RNA to stabilize complexes and manipulate local RNA structure.
Conclusion: AUF1 uses several molecular determinants to bind and remodel RNA targets.
Significance: This model explains AUF1 interactome diversity and predicts allosteric effects on protein and microRNA *trans*-factor binding to proximal sites.

AU-rich element RNA-binding protein 1 (AUF1) regulates the stability and/or translational efficiency of diverse mRNA targets, including many encoding products controlling the cell cycle, apoptosis, and inflammation by associating with AU-rich elements residing in their 3′-untranslated regions. Previous biochemical studies showed that optimal AUF1 binding requires 33–34 nucleotides with a strong preference for U-rich RNA despite observations that few AUF1-associated cellular mRNAs contain such extended U-rich domains. Using the smallest AUF1 isoform ($p37^{AUF1}$) as a model, we employed fluorescence anisotropy-based approaches to define thermodynamic parameters describing AUF1 ribonucleoprotein (RNP) complex formation across a panel of RNA substrates. These data demonstrated that 15 nucleotides of AU-rich sequence were sufficient to nucleate high affinity $p37^{AUF1}$ RNP complexes within a larger RNA context. In particular, $p37^{AUF1}$ binding to short AU-rich RNA targets was significantly stabilized by interactions with a 3′-purine residue and largely base-independent but non-ionic contacts 5′ of the AU-rich site. RNP stabilization by the upstream RNA domain was associated with an enhanced negative change in heat capacity consistent with conformational changes in protein and/or RNA components, and fluorescence resonance energy transfer-based assays demonstrated that these contacts were required for $p37^{AUF1}$ to remodel local RNA structure. Finally, reporter mRNAs containing minimal high affinity $p37^{AUF1}$ target sequences associated with AUF1 and were destabilized in a $p37^{AUF1}$-dependent manner in cells. These findings provide a mechanistic explanation for the diverse population of AUF1 target mRNAs but also suggest how AUF1 binding could regulate protein and/or microRNA binding events at adjacent sites.

Cellular homeostasis and function are intimately coupled to the precise control of gene expression. Accordingly, cells can regulate expression of specific genes at many levels, giving them strict control over the timing, abundance, and location of encoded gene products. For any protein coding gene, a key parameter contributing to the rate of protein production is the cytoplasmic concentration of its mRNA, which is established by the relative rates of mRNA synthetic processes including transcription, pre-mRNA processing, and nucleocytoplasmic transport, countered by the rate of cytoplasmic mRNA degradation (for review, see Refs. 1 and 2). Although cytoplasmic decay mechanisms regulate levels of all mRNAs, turnover kinetics vary widely across the cellular mRNA population. Gene-specific control of mRNA decay is mediated by *cis*-acting sequences located within each transcript, frequently localized to the 3′-untranslated region (3′-UTR). A prototypical family of mRNA stability determinants are the AU-rich elements (AREs)[3] frequently found in the 3′-UTRs of mRNAs encoding oncoproteins, cytokines, and inflammatory mediators (for review, see Ref. 3). AREs normally consist of a U-rich domain and frequent include one or more AUUUA pentamers, which genomic analysis indicates may occur in 5–8% of all human mRNAs (4).

The ability of AREs to control mRNA decay kinetics is governed by their association with cytoplasmic *trans*-acting factors, which may include both protein and nucleic acid components (2, 5). For example, binding by members of the Hu family of proteins including the ubiquitously expressed HuR stabilizes ARE-containing mRNAs, whereas recruitment of tristetraprolin, KSRP, or the microRNA miR-16 is associated with accelerated mRNA decay (2, 5, 6). However, for the AUF1 family of RNA-binding proteins, the biochemical and functional conse-

* This work was supported, in whole or in part, by National Institutes of Health Grant R01 CA102428 (NCI; to G. M. W.).
[1] Supported by American Heart Association Grant 11PRE6900008 and National Institutes of Health Grant T32 GM066706.
[2] To whom correspondence should be addressed: Dept. of Biochemistry and Molecular Biology, University of Maryland School of Medicine, 108 N. Greene St., Baltimore, MD. Tel.: 410-706-8904; Fax: 410-706-8297; E-mail: gwilson@som.umaryland.edu.

[3] The abbreviations used are: ARE, AU-rich element; AUF1, AU-rich element RNA-binding protein 1; Cy3, cyanine-3; Fl, fluorescein; RNP, ribonucleoprotein; hnRNP, heterogeneous nuclear RNP; PTB, polypyrimidine tract-binding protein; RRM, RNA recognition motif; βG, β-globin; RNP-IP, RNP immunoprecipitation; qRT-PCR, quantitative reverse transcription PCR; nt, nucleotide(s); EGFP, enhanced GFP; Dox, doxycycline.

quences of mRNA substrate binding appear to be more complex. AUF1 is encoded by a single copy gene on chromosome 4q21 that generates four protein isoforms via alternative pre-mRNA splicing (7), named according to their apparent molecular weights as $p37^{AUF1}$, $p40^{AUF1}$, $p42^{AUF1}$, and $p45^{AUF1}$. All isoforms contain two adjacent, centrally positioned RNA recognition motifs (RRMs) followed by a glutamine-rich domain. The $p37^{AUF1}$ and $p40^{AUF1}$ isoforms lack a 49-amino acid sequence near the C terminus encoded by exon 7, whereas $p37^{AUF1}$ and $p42^{AUF1}$ lack a 19-amino acid domain immediately N-terminal of RRM1 that is encoded by exon 2. However, although sharing common canonical RNA binding domains, the various AUF1 isoforms exhibit distinct subcellular localization profiles (8–11), diverse RNA binding affinities and effects on the structure of RNA ligands (12), and isoform-specific influences on the decay of mRNA targets (13–17).

All AUF1 isoforms form dimers in solution that can bind sequentially to RNA substrates to generate oligomeric ribonucleoprotein (RNP) structures (12, 18). To date, most biochemical characterization of RNA recognition by AUF1 has focused on RNA substrates derived from extended, contiguous ARE sequences such as those from the 3′-UTRs of mRNAs encoding tumor necrosis factor α (TNFα) or c-*fos* or similarly sized polyuridylate ligands (18–21). Although these studies have revealed many features regarding the mechanism and energetics of AUF1 RNP assembly, several details from these and other reports highlight deficiencies in our understanding of the RNA sequence requirements for high affinity AUF1 binding. First, using macromolecular binding density analysis, we recently demonstrated that the initial dimer binding event for either $p37^{AUF1}$ or $p42^{AUF1}$ occupies 33–34 nucleotides of RNA (12). Binding assays using truncated ARE substrates confirmed this as the lower size limit for high affinity AUF1 binding. This is a surprisingly large RNA footprint given that HuR, which contains three RRMs that contribute variously to its RNA binding activity, binds ARE substrates as small as 15 nt with low nanomolar affinity (22). A more analogous comparison might be the RNA binding domain of heterogeneous nuclear ribonucleoprotein (hnRNP) A1, which like AUF1 also contains two RRMs and forms dimers but interacts with only 11 nt of nucleic acid in each heteromolecular binding cleft (23). Second, transcripts containing >30 nt of contiguous AU-rich sequence are rare (24). Consistent with this, screening efforts have identified hundreds of AUF1-targeted mRNAs among the cellular transcript population but with few containing 3′-UTR sequences of 30 nt that consist solely of A and U residues (25, 26) and to date have not delineated precise RNA requirements for high affinity AUF1 binding. Together these data suggest that only a subset of AUF1-associated RNA nucleotides need be AU-rich to nucleate assembly of functional RNP complexes.

In this study we have tested the hypothesis that, although AUF1 binding must be nucleated by base-specific contacts involving a U-rich RNA domain, stabilization of AUF1 RNP complexes also requires base-independent contacts with flanking RNA sequences. The $p37^{AUF1}$ isoform was used as a model for these experiments because it binds ARE substrates with the highest affinity (12) and is most closely associated with destabilization of ARE-containing mRNA targets (15, 27). Fluorescence-based assay systems permitted quantitative assessment of the thermodynamic contributions of RNA ligand subdomains to AUF1 RNP assembly and local RNA structural remodeling, whereas cultured cell models were used to determine whether minimal high affinity AUF1 binding sites were functional. Findings from these experiments provide an explanation for the 3′-UTR sequence heterogeneity observed among AUF1-targeted mRNAs but also suggest potential mechanisms for cooperative or competitive relationships between AUF1 and other *trans*-acting factors for mRNA targets.

EXPERIMENTAL PROCEDURES

RNA Substrates—RNA oligonucleotides were synthesized, 2′-hydroxyl-deprotected, and purified by Integrated DNA Technologies, Dharmacon, or Sigma. Lyophilized pellets were resuspended in 10 mM Tris (pH 8.0). RNA concentrations and fluorophore labeling efficiencies were quantified by absorbance, incorporating fractional contributions from fluorescein (Fl) and/or cyanine-3 (Cy3) labels to A_{260} as described (20, 28). RNA probe sequences are listed in Table 1. Sequences denoted "ARE_{xx}" correspond to fragments of the core ARE from the 3′-UTR of TNFα mRNA. "$R\beta_{xx}$" sequences are derived from a non-AU-rich fragment from the coding sequence of rabbit β-globin mRNA. RNA substrates named with "Fl" and/or "Cy3" affixes denote the presence and location of the indicated fluorophore. Where indicated, 5′-hydroxyl RNA probes were radiolabeled with [γ-^{32}P]ATP by T4 polynucleotide kinase to a specific activity of $3–5 \times 10^3$ cpm/fmol as previously described (18).

Preparation of Recombinant AUF1 Proteins—Plasmid pBAD/HisB-$p37^{AUF1}$ was described previously (29) and expressed in Rosetta 2 *Escherichia coli* cells (Novagen). Recombinant His_6-$p37^{AUF1}$ protein was purified from cell lysates using Ni^{2+} affinity chromatography as previously described (12) except that buffer exchange into 10 mM Tris (pH 8.0) and protein concentration were both performed in Ambion ultracentrifugal filters. Recombinant protein purity and yield were assessed by Coomassie Blue-stained SDS-PAGE against a titration of bovine serum albumin.

Plasmids and Cell Lines—Plasmids expressing AUF1 and control short hairpin RNAs (shRNAs) were a gift from Dr. Gary Brewer. The expressed AUF1 shRNA targets a sequence encoded by exon 3, which is common to all isoforms (30). The plasmids were transfected into both HeLa and HeLa/Tet Off cell lines (Clontech) with Attractene transfection reagent, and stably expressing cell clones were selected with 400 μg/ml hygromycin B (Calbiochem). After selection, amplification, and screening, shAUF1 or shControl clonal cell lines were maintained by adding 100 μg/ml hygromycin B to regular growth media. Plasmid pcDNA/shR-$p37^{AUF1}$-FLAG encodes a C-terminal FLAG-tagged shRNA-resistant $p37^{AUF1}$, constructed by transferring the modified $p37^{AUF1}$ sequence from plasmid shR-$p37^{AUF1}$ (a gift from Dr. Gary Brewer; Ref. 31) into plasmid pcDNA3.1$^+$-FLAG (generously donated by Dr. Bret Hassel) using standard subcloning techniques. Mammalian β-globin (βG) reporter plasmids pTRERβ-wt and pTRERβ-ARE_{38} were described previously (21). Plasmid pTRERβ-RAR was constructed by inserting a DNA duplex encoding the $R\beta_{17}$-ARE_{16}-

TABLE 1
RNA substrates used in this study

Name	Sequence (5′ → 3′)[a]
ARE_{38}	GUGAUUAUUUAUUAUUUAUUUAUUAUUUAUUUAUUUAG
ARE_{24}	AUUUAUUUAUUAUUUAUUUAUUUA
ARE_{16}	AUUAUUUAUUUAUUUA
ARE_{15}	UUAUUUAUUUAUUUA
$R\beta_{17}$-ARE_{16}-$R\beta_{17}$	CCUGGCUCACAAAUACCAUUAUUUAUUUAUUUACCCUGGCUCACAAAUAC[b]
$R\beta_{17}$-ARE_{14}-$R\beta_{17}$	CCUGGCUCACAAAUACCUUAUUUAUUUAUUUCCCUGGCUCACAAAUAC
$R\beta_{17}$-ARE_{12}-$R\beta_{17}$	CCUGGCUCACAAAUACCUAUUUAUUUAUUCCCUGGCUCACAAAUAC
ARE_{15}-G	UUAUUUAUUUAUUUAG
ARE_{15}-A	UUAUUUAUUUAUUUAA
ARE_{15}-U	UUAUUUAUUUAUUUAU
ARE_{15}-C	UUAUUUAUUUAUUUAC
ARE_{15}-G-$R\beta_{13}$	UUAUUUAUUUAUUUAGGCUCACAAAUACC
$R\beta_{19}$-ARE_{15}-G	CCCCUGGCUCACAAAUACCUUAUUUAUUUAUUUAG
C_{19}-ARE_{15}-G	CCCCCCCCCCCCCCCCCCCCUUAUUUAUUUAUUUAG
$R\beta_{14}$-ARE_{15}-G	GGCUCACAAAUACCUUAUUUAUUUAUUUAG
$R\beta_{8}$-ARE_{15}-G	CAAAUACCUUAUUUAUUUAUUUAG
$R\beta_{4}$-ARE_{15}-G	UACCUUAUUUAUUUAUUUAG
$R\beta_{8}$-ARE_{15}	CAAAUACCUUAUUUAUUUAUUUA
ARE_{19}-G	UUUAUUAUUUAUUUAUUUAG
$R\beta_{31}$	UGGCCAAUGCCCUGGCUCACAAAUACCACUG

[a] RNA substrate variants containing 5′-linked Cy3 or Fl groups are indicated by relevant prefixes where applicable throughout the text. Similarly, RNA substrates containing 3′-fluorescein groups are suffixed by "Fl".
[b] For chimeric RNA substrates containing both ARE and non-ARE domains, the ARE sequences are underlined.

$R\beta_{17}$ RNA substrate (Table 1) into the BglII site of pTRERβ-wt, thus positioning the $R\beta_{17}$-ARE_{16}-$R\beta_{17}$ sequence within the reporter mRNA 3′-UTR. All plasmid constructs were verified by restriction digest and automated sequencing.

Measurements of RNA-Protein Binding—The number of RNP complexes formed between AUF1 and selected RNA substrates was monitored using electrophoretic mobility shift assays (EMSA) essentially as described (32). Briefly, ^{32}P-labeled RNA (0.2 nM) was incubated for 15 min on ice with increasing concentrations of His_6-$p37^{AUF1}$ in protein binding buffer (10 mM Tris-HCl (pH 8.0) containing 50 mM KCl, 2 mM DTT, 0.5 mM EDTA, 0.1 μg/μl acetylated bovine serum albumin, and 1 μg/μl heparin) plus 10% glycerol. Reaction components were resolved by electrophoresis through 6% native acrylamide gels run at 4 °C. Gels were dried, and products were visualized using Typhoon FLA-9500 phosphorimaging (GE Healthcare).

Quantitative assessments of AUF1-RNA binding equilibria were performed using fluorescence anisotropy essentially as described (12, 18, 29). Binding reactions (100 μl) were assembled as described for EMSAs but in buffer lacking glycerol and using Fl-labeled rather than radiolabeled RNA substrates. Reactions were incubated at 25 °C for 1 min based on kinetic runs, which verified that equilibrium is attained within this time frame (Refs. 18 and 33 and data not shown). Subsequently, total reaction anisotropy (A_t) and fluorescence intensity were measured using a Beacon 2000 Fluorescence Polarization System (Panvera) equipped with a 490-nm excitation filter and a 535-nm emission filter.

For most protein-RNA binding events, fluorescence intensity did not significantly vary as a function of protein concentration indicating similar quantum yields for all fluorescent reaction components. In these cases, measured anisotropy is proportional to the fractional concentrations of each fluorescent species at constant temperature and viscosity (34, 35). For RNA substrates where two $p37^{AUF1}$ dimers can bind to form a tetrameric $p37^{AUF1}$-RNA complex, the observed dissociation constants describing the first ($K_{d1\text{-}obs}$) and second ($K_{d2\text{-}obs}$) $p37^{AUF1}$ dimer binding steps are resolved by nonlinear regression of A_t as a function of protein dimer concentration ($[P_2]$) using Equation 1, where $K_{dx\text{-}obs} = 1/K_x$.

$$A_t = \frac{A_R + A_{P2R}K_1[P_2] + A_{P4R}K_1K_2[P_2]^2}{1 + K_1[P_2] + K_1K_2[P_2]^2} \quad \text{(Eq. 1)}$$

Here, A_R is the intrinsic anisotropy of the free RNA ligand, whereas A_{P2R} and A_{P4R} represent the intrinsic anisotropy values for AUF1 dimer-bound and AUF1 tetramer-bound RNA substrates, respectively. In cases where only a single AUF1 dimer binding event is indicated, this function is simplified by insertion of $K_2 = 0$ to yield Equation 2,

$$A_t = \frac{A_R + A_{P2R}K[P_2]}{1 + K[P_2]} \quad \text{(Eq. 2)}$$

However, for a subset of binding experiments involving short RNA ligands, fluorescence intensity was not constant across the tested range of His_6-$p37^{AUF1}$ concentrations, indicating that the quantum yields of the free RNA ligand (q_R) and the His_6-$p37^{AUF1}$ dimer-bound substrate (q_{P2R}) were not equivalent. In these cases the variations in quantum yield result in unequal contributions from bound and free RNA substrates to A_t. Lundblad *et al.* (36) described a function to calculate the bound substrate fraction (F_b) under conditions where the quantum yield of free and bound substrate varied. Adapted to our nomenclature, this function is given as Equation 3,

$$F_b = \frac{A_t - A_R}{(A_{P2R} - A_t)\left(\frac{q_{P2R}}{q_R}\right) + A_t - A_R} \quad \text{(Eq. 3)}$$

For single AUF1 dimer binding to RNA, $F_b = [P_2R]/[RNA]_{total}$. Substituting this and the conservation of mass function $[RNA]_{total} = [RNA]_{free} + [P_2R]$ into Equation 3 and solving for A_t in terms of the AUF1 dimer concentration $[P_2]$ yields Equation 4. For simplification, the term f_q has been substituted as the ratio of the fluorescence quantum yields of bound and free RNA substrates ($= q_{P2R}/q_R$). If the fluorescence intensity of Fl-tagged

RNA substrates does not vary as a result of protein binding, then $f_q = 1$, which simplifies Equation 4 to yield Equation 2.

$$A_t = \frac{A_R + A_{P2R}K[P_2]f_q}{1 + K[P_2]f_q} \quad \text{(Eq. 4)}$$

Equation 4 was used to analyze all RNA binding isotherms where total fluorescence intensity varied by >20%. In these cases, f_q was calculated by dividing the fluorescence intensity for the saturated protein-bound RNA complex (q_{P2R}) by the fluorescence intensity of the RNA substrate in the absence of protein (q_R).

Thermodynamic Parameters Contributing to AUF1 RNP Complex Formation—The contributions of changes in enthalpy ($\Delta H°$) and entropy ($T\Delta S°$) to the free energy of His_6-$p37^{AUF1}$ binding ($\Delta G°$) to selected RNA targets were resolved using van't Hoff analyses. Briefly, observed equilibrium association constants (K_{obs}) for His_6-$p37^{AUF1}$ binding to selected RNA substrates at various temperatures (T) between 5 and 37 °C were measured by fluorescence anisotropy as described above and then plotted as $\ln K_{obs}$ *versus* $1/T$. If $\Delta H°$ is constant across the temperature range tested, this plot will be linear and can be resolved using Equation 5, with 1.987×10^{-3} kcal·mol^{-1}·K^{-1} as the universal gas constant (R) (37, 38).

$$\ln K_{obs} = -\left(\frac{\Delta H°}{RT}\right) + \left(\frac{\Delta S°}{R}\right) \quad \text{(Eq. 5)}$$

However, when these plots are nonlinear, the contributions of enthalpy and entropy to binding free energy are no longer constant with temperature. In these cases, $\ln K_{obs}$ *versus* $1/T$ data sets were resolved using Equation 6, returning the change in molar heat capacity ($\Delta C°_{P,obs}$) and critical temperatures T_H and T_S, at which enthalpy and entropy, respectively, contribute no net energy to formation of AUF1 RNP complexes (38).

$$\ln K_{obs} = \left(\frac{\Delta C°_{P,obs}}{R}\right)\left(\left(\frac{T_H}{T}\right) - \ln\left(\frac{T_S}{T}\right) - 1\right) \quad \text{(Eq. 6)}$$

Solution of these parameters then allowed calculation of enthalpic and entropic contributions at any given temperature using Equations 7 and 8 (38).

$$\Delta H° = \Delta C°_{P,obs}(T - T_H) \quad \text{(Eq. 7)}$$

$$T\Delta S° = T\Delta C°_{P,obs}\cdot\ln\left(\frac{T}{T_S}\right) \quad \text{(Eq. 8)}$$

Analysis of Ionic Contributions to AUF1 RNP Assembly—Due to the highly negative charge on nucleic acid backbones, ions can be a significant factor driving the formation of protein-nucleic acid complexes, dominated by the release of cations from the nucleic acid. For a single protein (P) binding event on RNA (R) this equilibrium can be expressed using Equation 9.

$$P + R \rightleftharpoons PR + Z\psi M^+ \quad \text{(Eq. 9)}$$

Here, $Z\psi M^+$ represents the ions that are released as a result of ion bridges formed between the protein and nucleic acid that neutralize backbone phosphates (39). Specifically, ψ denotes the fraction of monovalent countercation (M^+) associated with the RNA per phosphate that approximates the axial charge density of the nucleic acid, and Z is the number of ion pairs formed between the RNA and protein. In this manner, the protein can be considered as a Z-valent ligand that neutralizes Z phosphates on RNA (40, 41). Following Le Chatelier's principle, the observed association constant between protein and RNA (K_{obs}) can thus be modulated by changes in the concentration of solution monovalent cation ($[M^+]$) using Equation 10,

$$K_{obs} = \frac{[PR][M^+]^{Z\psi}}{[R][P]} \quad \text{(Eq. 10)}$$

Incorporating K_T as the association constant at 1 M salt and taking logarithms yields Equation 11,

$$\log K_{obs} = \log K_T + Z\psi \log[M^+] \quad \text{(Eq. 11)}$$

When linear, the slope of a $\log K_{obs}$ *versus* $\log[M^+]$ plot can thus resolve Z if ψ is known. ψ is related to a parameter termed ξ, which is sequence-, pH-, and counterion-dependent and proportional to the structural charge density (42, 43). For polyU RNA, the value for ξ^{-1} has been measured as 0.615 (44), thus resolving $\psi = 1 - (2\xi)^{-1} = 0.693$ (43).

However, a nonlinear relationship between $\log K_{obs}$ and $\log[M^+]$ indicates that the displacement of cations from nucleic acid is not the only ionic event occurring upon protein binding. To account for these broader effects of ionic strength on RNP formation, we employed a counterion binding model derived by the Record (45) and Lohman (43) laboratories as adapted by Stickle and Fried (46, 47). This model includes changes in the numbers of protein-associated cations (Δm) and anions (Δn) resulting from protein binding to the nucleic acid target in addition to the change in cations associated with the nucleic acid (Δq). Incorporating these terms into Equation 11 and using [MX] in place of $[M^+]$ to indicate consideration of both cations and anions from the salt yields Equation 12 (45, 47).

$$\log K_{obs} = \log K_T + (\Delta m + \Delta n + \Delta q)\log[MX] \quad \text{(Eq. 12)}$$

Langmuir isotherms in Equation 13 model the change in cation association with the protein upon binding RNA based on differences in the average concentration of cation near the RNA ($[M^+]_R$) *versus* the bulk salt concentration ([MX]) where $K_d^{M^+}$ is the population averaged dissociation constant for cation to protein (47).

$$\Delta m = m_{tot}\left(\frac{[M^+]_R}{[M^+]_R + K_d^{M^+}} - \frac{[MX]}{[MX] + K_d^{M^+}}\right) \quad \text{(Eq. 13)}$$

The parameter m_{tot} is the number of cation binding sites transferred from the bulk solution to the RNA environment upon assembly of the RNP complex. Because $[M^+]_R$ is largely independent of bulk salt concentration between 10 mM to 1 M salt and $[M^+]_R \gg K_d^{M^+}$ (47), substituting Equation 13 into Equation 12 and simplifying yields Equation 14,

$$\log K_{obs} = \log K_T + \left(m_{tot}\left(1 - \frac{K_a^{M^+}[MX]}{1 + K_a^{M^+}[MX]}\right) + \Delta t\right)\log[MX]$$

(Eq. 14)

Here, Δt represents an aggregate ion release stoichiometry where $\Delta t = \Delta n + \Delta q$ and $K_a^{M^+} = 1/K_d^{M^+}$ (46). To define ionic contributions to the stability of His_6-$p37^{AUF1}$ RNP complexes, observed equilibrium binding constants (K_{obs}) were calculated from fluorescence anisotropy-based binding assays across a range of KCl concentrations (25–500 mM) and plotted as log K_{obs} *versus* log[KCl]. Values of logK_T, m_{tot}, $K_a^{M^+}$, and Δt were resolved by nonlinear regression to Equation 14.

Analysis of RNA Folding Using Fluorescence Resonance Energy Transfer (FRET)—Protein-induced changes in the global structure of RNA substrates were monitored by alterations in the distance between 3′-Fl (donor) and 5′-Cy3 (acceptor) dyes appended to each RNA ligand using FRET essentially as described previously (12, 21). FRET efficiency (E_{FRET}) is related to the interfluorophore distance by Equation 15 where r denotes the scalar distance between the donor and acceptor, and R_0 is the Förster distance defined as that yielding $E_{FRET} = 0.5$ (48). For Fl and Cy3 linked to single-stranded nucleic acids, R_0 has been calculated as 55.7 Å (49).

$$E_{FRET} = R_0^6/(R_0^6 + r^6) \quad \text{(Eq. 15)}$$

RNA binding reactions with varying concentrations of His_6-$p37^{AUF1}$ were assembled as described for fluorescence anisotropy measurements but in paired samples containing RNA substrates (2 nM) labeled either with a 3′-Fl (donor alone) or both 3′-Fl and 5′-Cy3 dyes (donor-acceptor pair). Donor fluorescence from each sample was measured by excitation at 485 nm and emission at 520 nm or scanning from 500 to 620 nm (10-nm slit widths) using a Cary Eclipse fluorometer (Varian). Background fluorescence was measured from samples lacking RNA probe. Inner filter effects and photobleaching were insignificant under these conditions (data not shown). E_{FRET} was calculated from the fluorescence of the donor in the presence (F_{DA}) or absence (F_D) of the FRET acceptor using Equation 16, where f represents the labeling efficiency of the Cy3 acceptor dye for each double-labeled RNA ligand (21).

$$E_{FRET} = 1 - \left[\frac{F_{DA} - F_D(1-f)}{F_D f}\right] \quad \text{(Eq. 16)}$$

Antibodies—For Western blotting rabbit polyclonal anti-AUF1 antibody was purchased from Millipore. Horseradish peroxidase-conjugated anti-glyceraldehyde-3-phosphate dehydrogenase (anti-GAPDH), anti-FLAG, and secondary anti-rabbit IgG antibodies were from Sigma.

Ribonucleoprotein Immunoprecipitation (RNP-IP)—HeLa/shAUF1 cells were co-transfected with pcDNA/shR-$p37^{AUF1}$-FLAG, specific βG reporter plasmids encoding transcripts containing or lacking putative $p37^{AUF1}$-binding sites, and plasmid pEGFP-C1 (Clontech) to control for transfection efficiency. The amounts of transfected βG plasmids were optimized to yield similar steady-state reporter mRNA concentrations. RNP complexes containing FLAG-$p37^{AUF1}$ were then isolated from crude cell lysates by RNP-IP and precipitated RNA purified essentially as described (50, 51). Levels of βG reporter and EGFP mRNAs recovered in unfractionated cytoplasm and immunoprecipitated RNP complexes were measured by multiplex TaqMan quantitative reverse transcription PCR (qRT-PCR) using the iScript One-Step qRT-PCR Kit for Probes (Bio-Rad) programmed with βG amplification primers GTGAACTGCACTGTGACAAGC and ATGAGTAGACAGCACAATAACCAG, βG TaqMan probe Fl-CGTTGCCCAGGAGCCTGAAGTTCTCA-Black Hole Quencher 1, EGFP primers GCGACACCCTGGTGAACC and GATGTTGTGGCGGATCTTGAAG, and EGFP TaqMan probe Texas Red-CACCTTGATGCCGTTCTTCTGCTTGTCG-Black Hole Quencher 2 (all 5′ to 3′ and from Integrated DNA Technologies). βG reporter mRNA levels measured in each RNP-IP reaction were then normalized to EGFP mRNA levels and expressed as a fraction of the total input level of each reporter transcript as described (26).

mRNA Decay Assays—The decay rates of βG reporter mRNAs were measured using doxycycline (Dox) time courses essentially as described previously (51, 52). Briefly, HeLa/Tet-Off cells were cotransfected with plasmids encoding specific reporter transcripts and pEGFP-C1. After 48 h, transcription of βG mRNA was inhibited with Dox (2 μg/ml; Sigma). Cells were harvested at time points thereafter, and DNA-free RNA was purified using the NucleoSpin RNA II kit (Macherey-Nagel). βG reporter mRNA levels were quantified relative to EGFP mRNA at each time point by qRT-PCR using the iScript One-Step qRT-PCR Kit for Probes (Bio-Rad) as described above. The percentage of reporter mRNA remaining in each sample was plotted as a function of time after Dox treatment, and first order decay constants (k) were resolved by nonlinear regression. From this, the mRNA half-life ($t_{½}$) was calculated using $t_{½} = \ln 2/k$.

Statistical Analyses—All regression and statistical analyses were performed using PRISM v3.03 software (GraphPad). Comparisons between resolved thermodynamic parameters, mRNA recoveries by RNP-IP, and mRNA decay kinetics were done using the unpaired t test. For all regression analyses, the appropriateness of analytical binding models was evaluated by the coefficient of determination (R^2) and analyses of residual randomness. Pairwise comparisons between analytical binding or van't Hoff models were performed using the F test where indicated. In all cases differences yielding $p < 0.05$ were considered significant.

RESULTS

$p37^{AUF1}$ Binding to Short (≤ 16-nt) ARE Substrates Is Dramatically Stabilized by the Addition of Flanking non-ARE Sequences—Previously we showed that $p37^{AUF1}$ dimers bind sequentially with high affinity to ARE-based RNA substrates of 34 nt or more in length (12). Binding is substantially weaker on ARE substrates of 30 nt or less consistent with the $p37^{AUF1}$ dimer binding site size of 33 nt on RNA calculated using macromolecular binding density analysis (12). On ARE ligands ≥34 nt, His_6-$p37^{AUF1}$ dimer binding generates two distinct RNP complexes (Fig. 1*A*, *left panel*) consistent with the formation of AUF1 tetramers on these substrates (18). As noted previously, $p37^{AUF1}$ RNPs are retained relatively weakly by EMSA, particularly at the first (P_2R) binding event, likely because of the highly dynamic nature of these complexes (12, 18). However, a two-step model of His_6-$p37^{AUF1}$ RNP assembly on a 38-nt ARE ligand was further supported by resolution of fluorescence anisotropy isotherms using Equation 1 (Fig. 1*B*, *left panel*), which

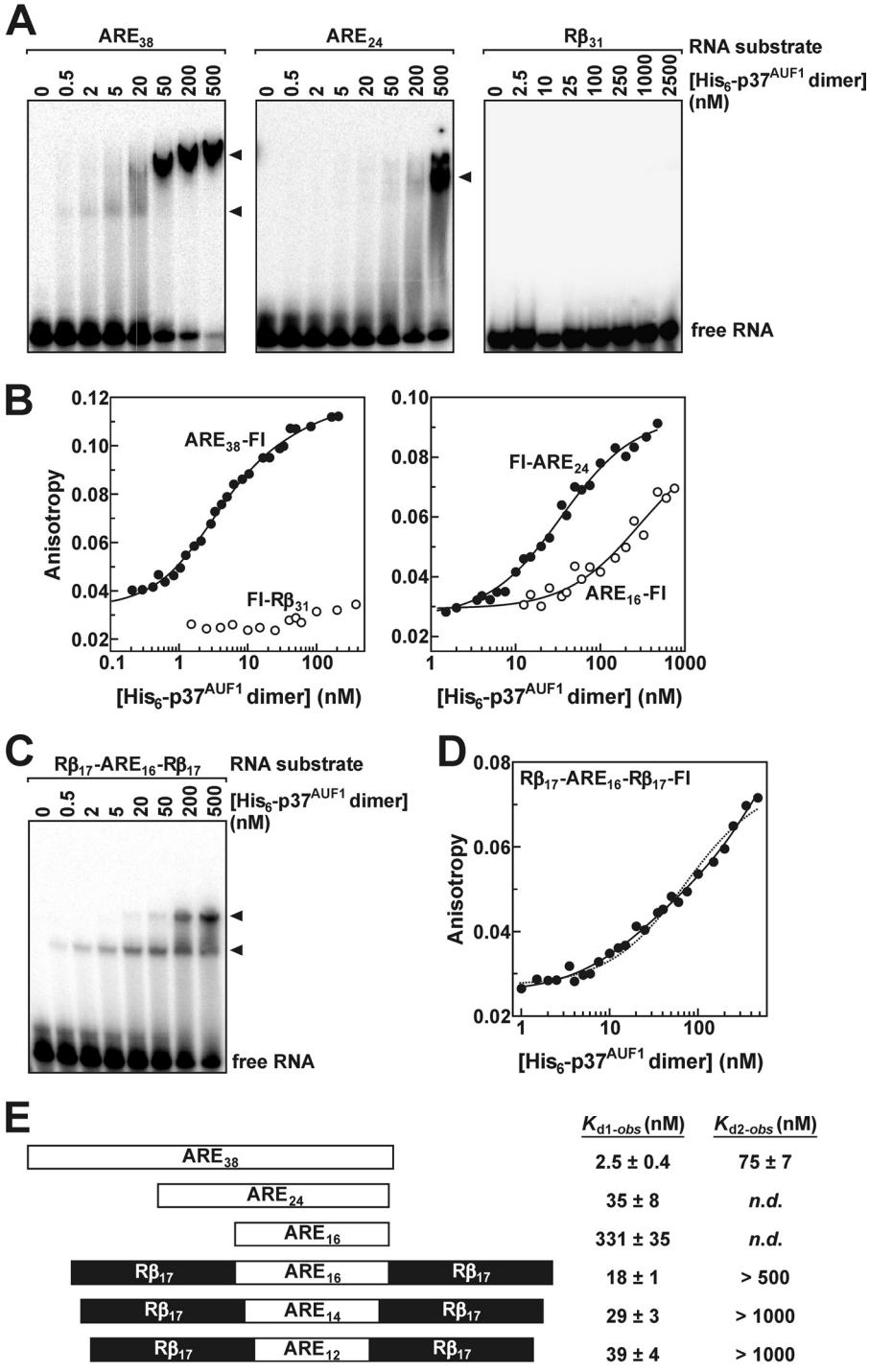

	$K_{d1\text{-}obs}$ (nM)	$K_{d2\text{-}obs}$ (nM)
ARE38	2.5 ± 0.4	75 ± 7
ARE24	35 ± 8	*n.d.*
ARE16	331 ± 35	*n.d.*
Rβ17-ARE16-Rβ17	18 ± 1	> 500
Rβ17-ARE14-Rβ17	29 ± 3	> 1000
Rβ17-ARE12-Rβ17	39 ± 4	> 1000

FIGURE 1. **p37^{AUF1} binding to ARE and chimeric RNA substrates.** *A*, analysis of His$_6$-p37^{AUF1} binding to indicated ^{32}P-labeled RNA ligands by EMSA. RNA-protein complexes formed are indicated by *black arrowheads*, whereas unbound probe is designated as *free RNA*. *B*, representative plots of His$_6$-p37^{AUF1} binding to the indicated Fl-tagged RNA substrates measured by fluorescence anisotropy. *Dots* indicate individual data points, whereas *solid lines* show optimal fits to a sequential two site binding model (*left*, Equation 1) or a single site binding model (*right*, Equation 2). *C*, EMSA analysis of His$_6$-p37^{AUF1} binding to ^{32}P-labeled RNA substrate Rβ_{17}-ARE$_{16}$- Rβ_{17}, with RNP complexes indicated by *black arrowheads*. *D*, representative fluorescence anisotropy plot of His$_6$-p37^{AUF1} binding to RNA ligand Rβ_{17}-ARE$_{16}$-Rβ_{17}-Fl with best fits to both a sequential two site binding model (*solid line*) and a single site model (*dotted line*). *E*, schematics of RNA substrates used in fluorescence anisotropy-based binding experiments show proportions and locations of ARE sequence (*open rectangles*) and non-ARE flanking domains (Rβ, *solid rectangles*). All RNA ligands included 5′- or 3′-Fl tags. Observed equilibrium dissociation constants describing the first ($K_{d1\text{-}obs}$) and second ($K_{d2\text{-}obs}$) His$_6$-p37^{AUF1} binding events are expressed as the mean ± S.D. of three independent experiments (*right*). *n.d.*, not detectable.

returns the observed dissociation constants describing both AUF1 dimer binding events. Conversely, shorter ARE ligands revealed only a single dimer binding event at protein concentrations up to 500 nM, both by EMSA (Fig. 1*A*, *center panel*) and resolution of anisotropy isotherms using the single site binding model described by Equation 2 (Fig. 1*B*, *right panel*), while calculated affinity constants affirm significant energetic penalties for His$_6$-p37^{AUF1} binding to shorter ARE substrates (Fig. 1*E*).

These data indicate that extended RNA substrates are required to stabilize formation of His_6-$p37^{AUF1}$ RNP complexes, far larger than the 9–15-nt RNA ligands needed to form stable complexes with HuR or the RNA binding domains of tristetraprolin or hnRNP A1 (22, 23, 53). However, they do not establish whether AUF1 binding is restricted to extended ARE substrates or if only a subset of the RNA ligand needs to be AU-rich to nucleate RNP assembly.

To discriminate between these possibilities, we assessed His_6-$p37^{AUF1}$ binding to a series of chimeric RNA substrates based on a 16-nt ARE flanked by sequences from a domain of the β-globin mRNA coding region ($R\beta_{31}$) that does not detectably bind His_6-$p37^{AUF1}$ (Fig. 1, *A*, *right panel*, and *B*, *left panel*). By fluorescence anisotropy, His_6-$p37^{AUF1}$ binding to the ARE_{16}-Fl substrate alone was weak but detectable (Fig. 1*B*, *right panel*). However, an RNA ligand incorporating 17 nt from the $R\beta_{31}$ sequence at both the 5′- and 3′-ends of the ARE_{16} substrate ($R\beta_{17}$-ARE_{16}-$R\beta_{17}$) formed two distinct RNP complexes with His_6-$p37^{AUF1}$ by EMSA (Fig. 1*C*), similar to the ARE_{38} substrate. Anisotropy-based binding assays also supported a two-step binding mechanism for the $R\beta_{17}$-ARE_{16}-$R\beta_{17}$-Fl ligand, as the single site model of Equation 2 yielded significant residual nonrandomness ($p = 0.006$; Fig. 1*D*, *dotted line*) and significantly increased sum-of-squares deviations relative to regression solutions based on the two-step binding model using the *F* test ($p < 0.0001$; Fig. 1*D*, *solid line*). However, although His_6-$p37^{AUF1}$ binding to the $R\beta_{17}$-ARE_{16}-$R\beta_{17}$ substrate demonstrated that extended ARE domains were not obligatory to form AUF1 tetrameric RNP complexes, more dramatic was the improvement in affinity of the initial His_6-$p37^{AUF1}$ dimer binding event ($K_{d1\text{-}obs}$), which was strengthened by nearly 20-fold for $R\beta_{17}$-ARE_{16}-$R\beta_{17}$ *versus* the ARE_{16} sequence alone (Fig. 1*E*). These data demonstrate that a smaller ARE sequence is sufficient to nucleate AUF1 RNP assembly if placed in a larger RNA context and that flanking nucleotides likely make base-independent contributions to the stability of AUF1 RNP complexes. However, shortening the ARE domain further weakened His_6-$p37^{AUF1}$ RNP formation (Fig. 1*E*).

A 3′ Purine and Nonspecific 5′ Nucleotides Significantly Stabilize $p37^{AUF1}$ Binding to a Minimal ARE Substrate—To define the features of non-ARE flanking sequences required to stabilize $p37^{AUF1}$ RNP assembly on a minimal ARE target, we measured the affinity of His_6-$p37^{AUF1}$ binding across a panel of RNA substrates by fluorescence anisotropy. Each RNA substrate was based on an ARE_{15} target for two reasons. First, its small size limits RNP complexes to a single AUF1 dimer, thus permitting the initial His_6-$p37^{AUF1}$ binding event to be effectively separated from subsequent formation of protein tetramers, which conceivably may be influenced by different RNA structural determinants. Second, His_6-$p37^{AUF1}$ binding to the ARE_{15}-Fl ligand is very weak in the absence of flanking sequence (Fig. 2), allowing us to accurately quantitate the contributions of adjacent RNA elements to RNP stability over an extended range.

Appending 14 nt of Rβ sequence to the 3′-end of the ARE_{15} substrate (ARE_{15}-G-$R\beta_{13}$-Fl) improved His_6-$p37^{AUF1}$ binding affinity nearly 12-fold ($\Delta\Delta G^\circ = -1.5$ kcal/mol; Fig. 2). Interestingly, limiting the 3′-flanking sequence to the initial base, a guanine, was sufficient to confer most of this RNP stabilizing

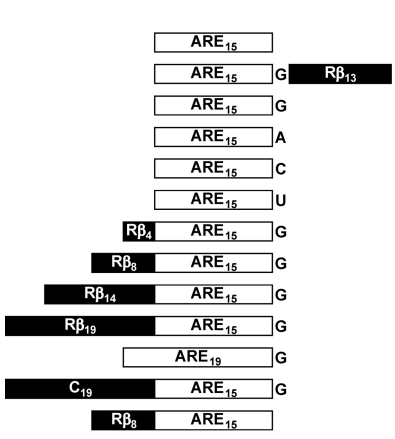

FIGURE 2. **Contributions of flanking non-ARE sequences to stability of $p37^{AUF1}$ RNPs.** Schematics of RNA substrates containing selected 5′- and/or 3′-sequences flanking a 15-nt core ARE domain (*open rectangles*). Extensions based on the Rβ sequence or polyC are shown by *solid rectangles*, whereas specific 3′-residues are labeled (*A*, *G*, *U*, or *C*). Observed equilibrium dissociation constants ($K_{d\text{-}obs}$) were resolved from anisotropy isotherms of Fl-tagged RNA ligands using Equation 2 or Equation 4 as described under "Experimental Procedures" and represent the mean ± S.D. from *n* independent experiments. Free energy of binding was calculated using $\Delta G^\circ = -RT\ln K_{obs}$ where *R* represents the gas constant (1.987×10^{-3} kcal·mol^{-1}·K^{-1}).

effect ($\Delta\Delta G^\circ = -1.1$ kcal/mol). The observation that the affinity of His_6-$p37^{AUF1}$ for the ARE_{15}-G-Fl substrate was significantly greater than that for ARE_{16}-Fl (Fig. 1*E*) suggested that contributions of this 3′-G residue to RNP stability may be base-specific. To test this possibility, His_6-$p37^{AUF1}$ binding was also measured to RNA substrates ARE_{15}-A-Fl, ARE_{15}-C-Fl, and ARE_{15}-U-Fl. Although neither the 3′-C nor U residues significantly enhanced protein binding affinity relative to ARE_{15}-Fl or ARE_{16}-Fl, His_6-$p37^{AUF1}$ bound the ARE_{15}-A-Fl substrate with an affinity identical to ARE_{15}-G-Fl, indicating that $p37^{AUF1}$ RNPs are stabilized specifically by a purine residue 3′ of the core ARE sequence. Conceivably, the purine base could directly interact with AUF1 or stabilize the complex through an allosteric mechanism.

To assess the contributions of non-ARE residues upstream of the ARE_{15} core, various lengths of Rβ sequence were appended to the 5′-end of the ARE_{15}-G-Fl substrate. The affinity of His_6-$p37^{AUF1}$ binding increased as a function of 5′-Rβ sequence length, with 19 nt ($R\beta_{19}$-ARE_{15}-G-Fl) improving protein affinity >5-fold ($\Delta\Delta G^\circ = -1.0$ kcal/mol). Experiments with two additional RNA substrates showed that both base-specific and non-base-specific interactions contribute to RNP stabilization by 5′-flanking sequences. First, adding 4 nt of Rβ sequence ($R\beta_4$-ARE_{15}-G-Fl) or 4 nt of ARE sequence (ARE_{19}-G-Fl) 5′ of ARE_{15}-G yielded essentially identical improvements in the affinity of His_6-$p37^{AUF1}$ binding (Fig. 2), indicating a base-independent effect on RNP stability. However, although the addition of 19 C residues upstream of ARE_{15}-G-Fl also significantly stabilized $p37^{AUF1}$ RNP formation (C_{19}-ARE_{15}-G-Fl; $\Delta\Delta G^\circ = -0.5$ kcal/mol), stabilization by the C_{19} domain was only half that observed with the 5′-$R\beta_{19}$ sequence, suggesting that some primary or potentially secondary structural features of the Rβ-based 5′-domain make additional contributions to His_6-$p37^{AUF1}$ binding.

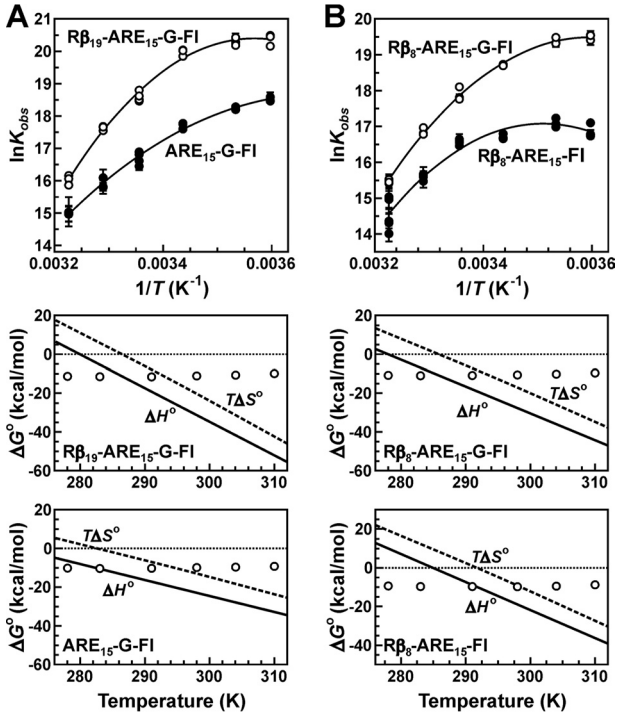

FIGURE 3. **Temperature dependence of p37^{AUF1} binding to RNA ligands.** Anisotropy-based binding assays containing His$_6$-p37^{AUF1} and the indicated Fl-tagged RNA substrates were performed across a range of reaction temperatures (5–37 °C). Observed association constants (K_{obs}) were resolved using Equation 2. *A*, van't Hoff plots of lnK_{obs} *versus* 1/*T*. Each point is derived from the value of K_{obs} calculated from an independent binding isotherm ± the S.E. of regression (approximately half of the 95% confidence interval) calculated by PRISM v3.03 software. Data sets generated using each RNA ligand were then fit using Equation 6. Resolved thermodynamic constants are listed in Table 2. *B*, enthalpic (Δ*H*°, *solid lines*) and entropic (*T*Δ*S*°, *dashed lines*) contributions to the stability of His$_6$-p37^{AUF1} complexes on each RNA ligand were calculated as a function of temperature using Equations 7 and 8, respectively. Changes in enthalpy and entropy contributed no net energy to Δ*G*° at their critical temperatures of T_H and T_S, respectively, indicated by the intersection of these functions with Δ*G*° = 0 (*dotted line*). The total free energy of RNP formation (Δ*G*°) was determined at each temperature using Δ*G*° = −*RT*lnK_{obs} (*open circles*).

5′- and 3′-Non-ARE Nucleotides Make Distinct Thermodynamic Contributions to p37^{AUF1} RNP Assembly—To identify thermodynamic features contributing to p37^{AUF1} RNP formation by sequences flanking the ARE$_{15}$ RNA ligand domain, enthalpic and entropic contributions to RNP stability were assessed using van't Hoff analyses. The role of the 5′ non-ARE domain was determined by comparing His$_6$-p37^{AUF1} binding to RNA substrates Rβ_{19}-ARE$_{15}$-G-Fl *versus* ARE$_{15}$-G-Fl. For ARE$_{15}$-G-Fl, a plot of lnK_{obs} *versus* 1/*T* appeared to show modest downward curvature (Fig. 3*A*, *top panel*). Fitting these data to the linear van't Hoff function described by Equation 5 yielded reasonably confident values for the enthalpic (Δ*H*°) and entropic (*T*Δ*S*°) contributions to binding energy, and a residual runs test did not indicate significant deviation from linearity ($p = 0.117$). However, an *F* test comparison of regression solutions to Equations 5 *versus* 6 strongly favored the latter model ($p < 0.0001$), and as such the thermodynamics of His$_6$-p37^{AUF1} binding to ARE$_{15}$-G-Fl RNA were interpreted using the nonlinear function. By this model, p37^{AUF1} binding to this RNA target is associated with a small but statistically significant negative change in heat capacity ($\Delta C°_{P,obs}$) (Table 2) and a corresponding temperature dependence of both Δ*H*° and *T*Δ*S*°. Solving these parameters as a function of temperature (Fig. 3*A*, *bottom panel*) revealed that, at all temperatures tested, His$_6$-p37^{AUF1} binding to the ARE$_{15}$-G-Fl ligand is driven by enthalpic effects (Δ*H*° < 0) and that above 10 °C, this must overcome unfavorable changes in system entropy (*T*Δ*S*° < 0). A negative $\Delta C°_{P,obs}$ is commonly seen in "induced fit" protein-nucleic acid binding mechanisms that involve conformational rearrangements within one or both binding partners (37, 53, 54).

By comparison, the negative curvature observed in the van't Hoff plot of His$_6$-p37^{AUF1} binding to RNA substrate Rβ_{19}-ARE$_{15}$-G-Fl was much more pronounced (Fig. 3*A*, *top panel*). These data resolved a significantly larger negative value for $\Delta C°_{P,obs}$ than that observed for p37^{AUF1} binding to the RNA ligand lacking the 5′-Rβ_{19} domain (Table 2), suggesting that upstream nucleotide contacts may induce new or more pronounced conformational changes within RNP complex constituents. Consistent with this model, there is a larger entropic penalty for p37^{AUF1} binding to Rβ_{19}-ARE$_{15}$-G-Fl compared with the ligand lacking the 5′-Rβ sequence (ARE$_{15}$-G-Fl) at 25 °C, although enhanced enthalpic contributions by the 5′-Rβ_{19} domain more than compensate for this (Table 2). The improvement in Δ*H*° associated with the 5′-Rβ_{19} domain is consistent with additional protein contacts involving this sequence, whereas the increased entropic penalty suggests that these contacts may limit conformational freedom near or solvent exclusion from the binding interface.

The effects of a 3′-purine residue on the energetic contributions to p37^{AUF1} RNP assembly were assessed using similar van't Hoff analyses but comparing His$_6$-p37^{AUF1} binding to RNA ligands Rβ_8-ARE$_{15}$-Fl and Rβ_8-ARE$_{15}$-G-Fl (Fig. 3*B*). Comparisons were performed in the presence of the 8-nt 5′-Rβ sequence because very weak protein binding by the ARE$_{15}$-Fl ligand (Fig. 2) precluded accurate measurements of its affinity across the temperature range necessary to confidently resolve thermodynamic components of binding energy. The presence of the 3′-G residue did not significantly alter the negative value of $\Delta C°_{P,obs}$ associated with His$_6$-p37^{AUF1} binding but did enhance both the enthalpic benefit and entropic penalties of RNP assembly at 25 °C (Table 2), suggesting the formation of additional contacts between the protein and the 3′-terminal G.

A common base-independent mechanism that stabilizes protein binding to nucleic acids is through ionic interactions between positively charged functional groups on the protein and the negatively charged nucleic acid backbone (55–57). To determine whether new ionic contacts involving 5′-flanking sequences or a 3′-purine (using G as a model) stabilize p37^{AUF1} binding to ARE$_{15}$-containing RNA ligands, we measured the affinity of His$_6$-p37^{AUF1} for selected RNA substrates across a range of KCl concentrations, then plotted log K_{obs} *versus* log-[KCl]. Frequently, these analyses are well described by linear functions, as high solution cation concentrations compete with the protein for the negatively charged phosphodiester nucleic acid backbone (22, 53, 55, 58, 59). However, in all cases tested logK_{obs} displayed a multiphasic response to changes in log[KCl] (Fig. 4). In high salt, the RNA binding activity of His$_6$-p37^{AUF1} was weakened, consistent with competition for ion pairs contributing to RNP stability. However, under hypotonic condi-

TABLE 2

Thermodynamic contributions to p37^{AUF1} RNP formation on selected RNA substrates

RNA substrate	$\Delta C°_{P,obs}$ [a]	T_H [a]	T_S [a]	$\Delta H°$ at 25 °C [b]	$T\Delta S°$ at 25 °C [c]
	kcal/mol·K	*K*	*K*	*kcal/mol*	*kcal/mol*
Rβ_{19}-ARE$_{15}$-G-Fl	−1.77 ± 0.13	280.3 ± 1.1	286.8 ± 0.6	−31.4 ± 1.9	−20.2 ± 1.1
ARE$_{15}$-G-Fl	−0.83 ± 0.11	270.3 ± 3.1	282.7 ± 1.5	−22.9 ± 2.6	−13.0 ± 1.3
Rβ_8-ARE$_{15}$-G-Fl	−1.38 ± 0.08	278.0 ± 0.9	285.9 ± 0.5	−27.7 ± 1.3	−17.0 ± 0.7
Rβ_8-ARE$_{15}$-Fl	−1.45 ± 0.20	284.9 ± 1.4	291.7 ± 0.7	−19.0 ± 2.0	−9.2 ± 1.0

[a] For His$_6$-p37^{AUF1} binding to each RNA substrate, the observed change in molar heat capacity ($\Delta C°_{P,obs}$) and critical temperatures at which enthalpy (T_H) and entropy (T_S) make no contributions to binding free energy were resolved by nonlinear regression of van't Hoff plots using Equation 6 as shown in Fig. 3. Parameter values are given ±S.E. of regression (approximately half of the 95% confidence interval) calculated by PRISM v3.03 software.

[b] $\Delta H°$ at 25 °C was calculated using Equation 7.

[c] $T\Delta S°$ at 25 °C was calculated using Equation 8.

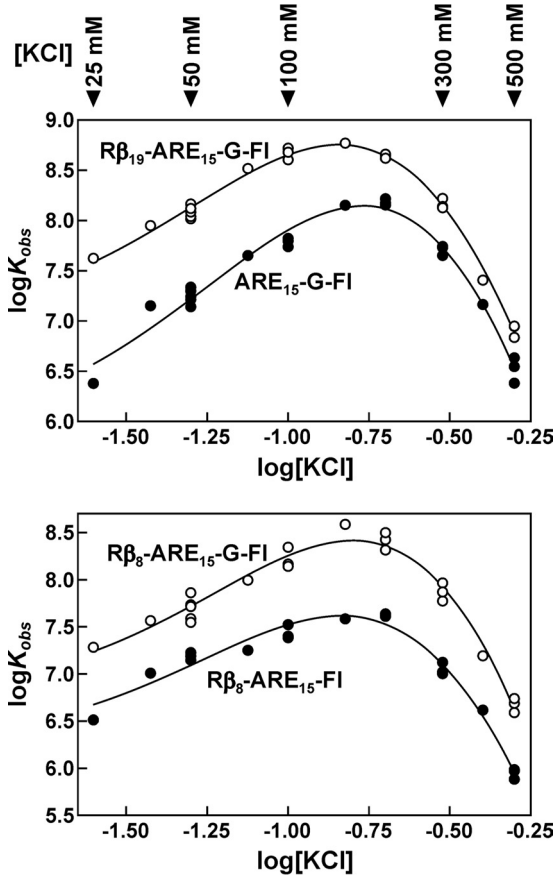

FIGURE 4. **Sensitivity of p37^{AUF1} RNP formation to ionic strength.** The affinity of His$_6$-p37^{AUF1} for the indicated RNA substrates was assayed across a range of KCl concentrations (25–500 mM) by fluorescence anisotropy. Points represent solutions of K_{obs} from each individual binding experiment resolved using Equation 2 and are plotted as logK_{obs} *versus* log[KCl]. Parameters describing ionic interactions with and contributions to the formation of His$_6$-p37^{AUF1} RNP complexes with each RNA ligand were resolved by nonlinear regression using Equation 14 (*solid lines*) and are listed in Table 3.

tions His$_6$-p37^{AUF1} binding was also impaired, suggesting that specific macromolecular interactions with ions in solution could also be required to stabilize p37^{AUF1} RNP complexes or to maintain the protein in an active conformation as has been postulated for binding of the *E. coli* CAP and AraC proteins to cognate DNA targets (46, 60). To incorporate broader roles for solvated ions in p37^{AUF1} RNP assembly, logK_{obs} *versus* log[KCl] plots were analyzed using a more inclusive counterion binding model described by Equation 14 (Fig. 4, *solid lines*). Among the resolved parameters, this model estimates the stoichiometry of ion release upon macromolecular binding (Δt), which is the sum of anions released from His$_6$-p37^{AUF1} and cations released

TABLE 3

Ionic contributions to p37^{AUF1} RNP formation on selected RNA substrates

For His$_6$-p37^{AUF1} binding to each RNA substrate the number of cation binding sites transferred from the bulk solution to the RNA environment upon assembly of the RNP complex (m_{tot}), the population averaged association constant of K^+ for His$_6$-p37^{AUF1} ($K_a^{M^+}$), the affinity constant of His$_6$-p37^{AUF1} for each RNA ligand (K_T), and the aggregate ion-release stoichiometry of anions from AUF1 and cations from the RNA (Δt) were resolved by nonlinear regression of logK_{obs} *versus* log[KCl] plots by Equation 14 as shown in Fig. 4. All parameter values are listed ± the S.E. of regression (approximately half of the 95% confidence interval) calculated by PRISM v3.03 software.

RNA substrate	m_{tot}	$K_a^{M^+}$	logK_T	Δt
		M^{-1}		
ARE$_{15}$-G-Fl	15 ± 2	3.1 ± 0.6	3.6 ± 0.4	−16 ± 3
Rβ_{19}-ARE$_{15}$-G-Fl	12 ± 1	3.9 ± 0.4	4.1 ± 0.2	−13 ± 1
Rβ_8-ARE$_{15}$-Fl	12 ± 2	3.4 ± 0.7	3.3 ± 0.3	−13 ± 2
Rβ_8-ARE$_{15}$-G-Fl	16 ± 3	2.9 ± 0.6	3.5 ± 0.4	−17 ± 3

from RNA (Table 3). An increase in ion pairs formed between His$_6$-p37^{AUF1} and an RNA substrate would thus be expected to increase the value of Δt, as localized counterions would be ejected from macromolecular binding partners during RNP assembly. Interestingly, neither the 5′-non-ARE sequences (Table 3, *cf.* ARE$_{15}$-G-Fl *versus* Rβ_8-ARE$_{15}$-G-Fl and Rβ_{19}-ARE$_{15}$-G-Fl) nor the 3′-G residue (*cf.* Rβ_8-ARE$_{15}$-Fl *versus* Rβ_8-ARE$_{15}$-G-Fl) significantly altered Δt, suggesting that the enhancements in RNP stability conferred by each flanking RNA domain do not require the formation of new ionic contacts with the protein. This was not unexpected for the enhanced affinity conferred by the 3′-purine because of its specificity for an A or G nucleobase. However, given that RNP stabilization by the 5′-Rβ-derived domains includes substantial base-independent components, these data suggest that non-ionic interactions, possibly including contacts with functional groups on ribose sugars or allosteric mechanisms, are primarily responsible for the contributions of 5′-flanking sequences to p37^{AUF1} binding.

Sequences 5′ of the Nucleating ARE Domain Are Required for p37^{AUF1}-induced Condensation of Local RNA Structure—The observation that adding Rβ-derived nucleotides 5′ of the ARE$_{15}$-G domain significantly increased the negative change in heat capacity upon His$_6$-p37^{AUF1} binding suggested that sequences upstream of ARE$_{15}$ may induce or enhance structural remodeling upon RNP formation. Conceivably, this could involve conformational changes in the protein and/or RNA moieties. However, given that we have previously reported a global condensation of local RNA structure associated with initial AUF1 dimer binding events for all isoforms (12, 20, 33), we investigated whether protein contacts 5′ of the core ARE$_{15}$

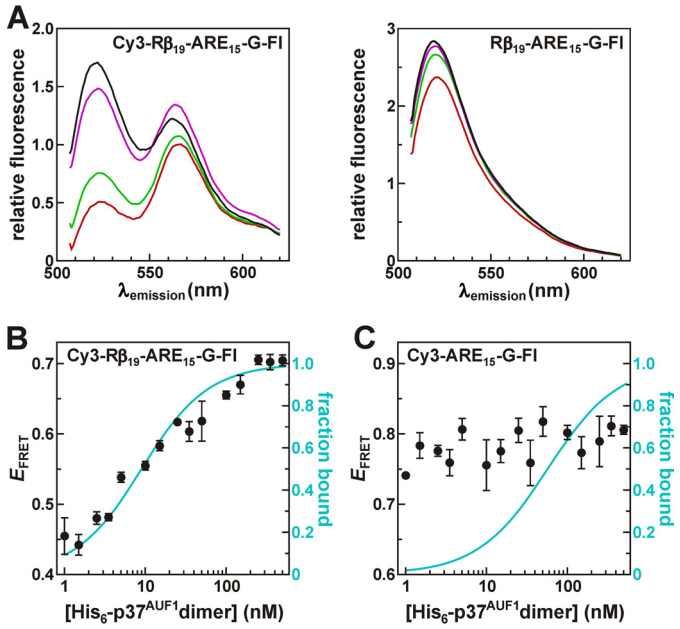

FIGURE 5. **Effect of p37^{AUF1} on the global structure of selected RNA substrates resolved using FRET.** *A*, blank-corrected fluorescence emission spectra of RNA substrate Rβ_{19}-ARE$_{15}$-G (2 nM) containing a 3′-Fl FRET donor dye with (*left panel*) or without (*right panel*) a 5′-Cy3 FRET acceptor, in the presence of 0 nM (*black line*), 2.5 nM (*violet*), 25 nM (*green*), or 250 nM (*red*) His$_6$-p37^{AUF1} dimer. His$_6$-p37^{AUF1}-dependent changes in the distance between the 5′ and 3′ termini of RNA ligands Cy3-Rβ_{19}-ARE$_{15}$-G-Fl (*B*) and Cy3-ARE$_{15}$-G-Fl (*C*) were determined by measuring FRET efficiency (E_{FRET}) between the Fl and Cy3 moieties of each substrate across titrations of His$_6$-p37^{AUF1} using Equation 16 as described under "Experimental Procedures." Data points represent the mean ± S.D. from three independent reactions. For comparison, the fraction of RNA ligand bound at each protein concentration (*blue line*) was determined using Equation 2 with equilibrium binding constants resolved from anisotropy experiments described in Fig. 2.

sequence were required for the RNA conformational remodeling activity of p37^{AUF1}.

Protein-dependent changes in the global conformation of RNA ligands were monitored by variations in FRET efficiency (E_{FRET}) between 3′-Fl and 5′-Cy3 fluorophores. For RNA substrate Cy3-Rβ_{19}-ARE$_{15}$-G-Fl, binding to His$_6$-p37^{AUF1} significantly decreased emission from the FRET donor (Fl) but only if the FRET acceptor (Cy3) was present (Fig. 5*A*, *cf.* emission at 520 nm in *left versus right panels*). Calculating E_{FRET} from measurements of Cy3-Rβ_{19}-ARE$_{15}$-G-Fl donor emission across a titration of His$_6$-p37^{AUF1} shows that the 5′- and 3′-termini of the RNA ligand are forced closer together upon binding the protein (Fig. 5*B*, *solid circles*). Furthermore, the protein concentration dependence of RNA structural remodeling parallels the fractional concentration of RNA within RNP complexes (Fig. 5*B*, *blue lines*). Conversely, an RNA ligand lacking the 5′-Rβ domain (Cy3-ARE$_{15}$-G-Fl) exhibited no change in the average distance between its 5′- and 3′-termini upon binding His$_6$-p37^{AUF1} (Fig. 5*C*). Together, these data indicate that local RNA remodeling by p37^{AUF1} involves contacts with sequences upstream of the nucleating ARE$_{15}$ domain and that these conformational changes may be a major contributor to the change in heat capacity observed during AUF1 RNP formation on these RNA targets. These findings are consistent with previous observations of AUF1-induced conformational changes in extended ARE and polyuridylate ligands (12, 20) but also indicate that condensation of local RNA structure is largely independent of the upstream sequence identity.

A Minimal p37^{AUF1}-binding RNA Substrate Is a Functional AUF1-regulated mRNA-destabilizing Element in Cells—Our previous report demonstrated that high affinity p37^{AUF1} binding required >34 nt of RNA (12). However, data from this study indicate that only a fraction of the AUF1-binding site on RNA requires AU-rich sequence and that a 15–16 nt ARE fragment can nucleate formation of stable (K_d < 20 nM) complexes with His$_6$-p37^{AUF1} *in vitro* when positioned within a larger RNA context. Accordingly, we tested whether a reporter mRNA containing a minimal high affinity p37^{AUF1}-binding site could be recognized and regulated by AUF1 in cells.

Stable HeLa and HeLa/Tet-Off cell lines were developed that expressed a non-targeting control shRNA (shControl) or one that targeted a domain common to all AUF1 mRNA variants (shAUF1). Western blots demonstrated robust suppression of all AUF1 protein isoforms in the shAUF1 lines (Fig. 6*A*). Transient transfection of a shRNA-resistant FLAG-tagged p37^{AUF1} expression plasmid into shAUF1 clonal lines permitted selective expression of the p37^{AUF1} isoform at near- or subphysiological levels (Fig. 6*A*, *right lane*), thus minimizing potential complications of protein overexpression. Into each of these cell backgrounds we also transfected reporter constructs under the control of Dox-responsive promoters, expressing either wild type βG mRNA (βG-wt) or βG containing the Rβ_{17}-ARE$_{16}$-Rβ_{17} sequence downstream of the translation termination codon (Fig. 6*B*, *βG-RAR*). An additional reporter mRNA included the 38-nt core ARE from TNFα mRNA (*βG-ARE$_{38}$*) as a positive control, as a previous study indicated that this transcript bound AUF1 and was stabilized in shAUF1-expressing cells (26).

In RNP-IP experiments, inclusion of either the ARE$_{38}$ or RAR sequences significantly enhanced reporter mRNA recovery in immunoprecipitates containing p37^{AUF1}-FLAG (Fig. 6*C*, p < 0.002 *versus* βG), indicating that both p37^{AUF1} binding determinants can associate with the cellular protein. We next tested whether expression of AUF1 modulated reporter mRNA decay kinetics in HeLa/Tet-Off cell models using Dox time course assays, as the canonical role of AUF1, particularly the p37^{AUF1} isoform, is to promote degradation of mRNA substrates (15, 61). βG-wt mRNA, which lacks any ARE sequences, decayed very slowly in HeLa/Tet-Off cells expressing either shControl or shAUF1 (Fig. 6*D*, *left panel*), resolving mRNA half-lives of greater than 10 h in each cell background (Table 4). As expected, insertion of the ARE$_{38}$ sequence into the 3′-UTR of βG mRNA shortened the mRNA half-life to 1 h in shControl-expressing cells (Fig. 6*D*, *center panel*), whereas suppression of endogenous AUF1 by shRNA stabilized βG-ARE$_{38}$ mRNA 2-fold. Inclusion of the RAR sequence in the 3′-UTR also significantly accelerated reporter mRNA decay but to a lesser extent than the ARE$_{38}$ sequence (Fig. 6*D*, *right panel*). However, decay of the βG-RAR mRNA was also regulated by AUF1, as this transcript was stabilized by ~60% in the shAUF1-expressing cell background (Table 4). Notably, expression of the shRNA-resistant p37^{AUF1}-FLAG completely reversed shAUF1-induced stabilization of both βG-ARE$_{38}$ and βG-RAR mRNAs. The results from these ectopic p37^{AUF1} rescue experiments

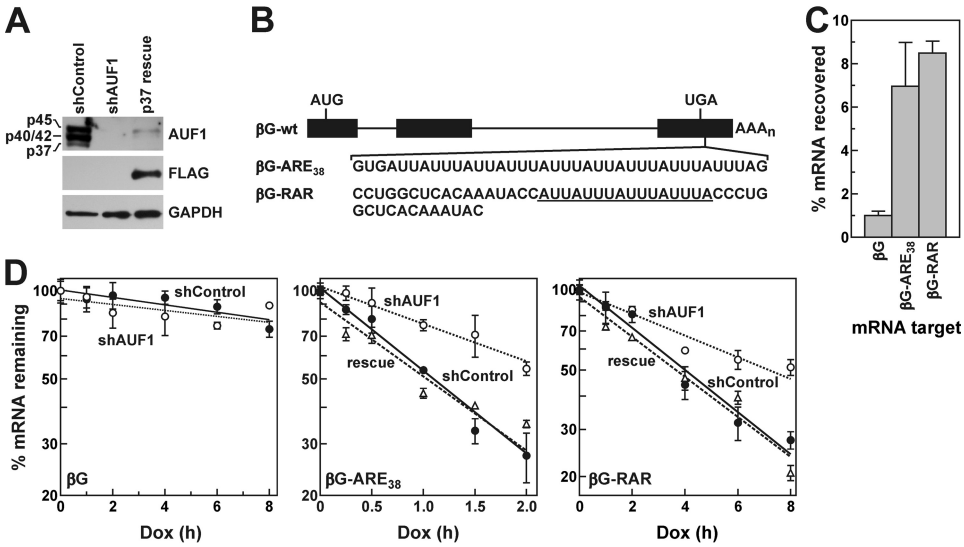

FIGURE 6. **p37^{AUF1} binding and destabilization of cellular ARE reporter mRNAs.** *A*, Western blots of endogenous AUF1 and ectopically expressed p37^{AUF1}-FLAG in whole-cell lysates from HeLa/Tet-Off clonal lines that stably express shAUF1 or a control shRNA and in the shAUF1 line co-transfected with pcDNA/shR-p37^{AUF1}-FLAG (*rescue*). GAPDH was used as a loading control. *B*, organization of the transcript expressed from the pTRERβ-wt reporter plasmid showing positions of exons (*black boxes*) and introns (*lines*). Inserting the core ARE sequence from TNFα mRNA or the Rβ_{17}-ARE$_{15}$-Rβ_{17} RNA sequence downstream of the βG translational termination codon generated βG-ARE$_{38}$ and βG-RAR, respectively. *C*, βG reporter mRNAs binding to p37^{AUF1}-FLAG were purified from HeLa cell lysates by immunoprecipitation with anti-FLAG antibody and quantified by qRT-PCR. *Bars* show yields of each reporter mRNA recovered in immunoprecipitates relative to total input levels of each reporter transcript and represent the mean ± S.D. of four qRT-PCR reactions. Triplicate independent experiments yielded similar results. *D*, representative Dox time course experiments measuring the decay kinetics of indicated reporter mRNAs in HeLa/Tet-Off cell models expressing shControl, shAUF1, or shAUF1 cells expressing FLAG-p37^{AUF1} as shown in *A*. Points indicate the mean ± S.D. of four qRT-PCR reactions at each time point. Data sets were resolved by nonlinear regression using a single exponential decay model to determine mRNA decay constants and associated half-lives. Averaged mRNA decay constants from multiple independent time course experiments are listed in Table 4.

TABLE 4
Effect of AUF1 on reporter mRNA decay kinetics

Reporter mRNA	shRNA	$t_{1/2}$[a]	*n*	*t* test comparisons
		h		
βG	shControl	>10 h	3	
	shAUF1	>10 h	3	
βG-ARE$_{38}$	shControl	1.01 ± 0.24	5	
	shAUF1	2.11 ± 0.33	4	$p = 0.0007$ *vs.* shControl
	shAUF1 + p37^{AUF1}-FLAG	1.09 ± 0.15	4	$p = 0.0014$ *vs.* shAUF1
βG-RAR	shControl	3.98 ± 0.11	3	
	shAUF1	6.34 ± 0.88	4	$p = 0.0062$ *vs.* shControl
	shAUF1 + p37^{AUF1}-FLAG	3.82 ± 0.62	3	$p = 0.0083$ *vs.* shAUF1

[a] Turnover kinetics of listed βG reporter mRNAs were measured in HeLa/Tet-Off cells expressing the indicated shRNAs or p37^{AUF1}-FLAG in an shAUF1-expressing background using Dox time course assays as described under "Experimental Procedures" and Fig. 6. Listed mRNA half-life values represent the mean ± S.D. from *n* independent time course experiments.

confirm that inhibition of reporter mRNA decay in shAUF1-expressing cells was not an off-target effect of RNA silencing and that near-physiological levels of the p37^{AUF1} isoform were sufficient to accelerate decay of each ARE-containing reporter mRNA. Together these data indicate that a minimal high affinity p37^{AUF1} target sequence forms RNP complexes with this AUF1 isoform that accelerate mRNA turnover in a cellular context.

DISCUSSION

The nucleotide determinants required for AUF1 binding to RNA targets control the affinity and positioning of AUF1 recruitment and by extension the biochemical and functional consequences of these interactions. Our previous work using macromolecular binding density analysis and truncated ARE substrates demonstrated that for p37^{AUF1} and p42^{AUF1}, association of the first protein dimer occupies 33–34 nucleotides of RNA (12). Shorter RNA ligands showed significantly weaker binding, whereas above this site size a second AUF1 dimer binding event became measureable (12). Data from the current study are consistent with this unusually large RNA site size required to form high affinity p37^{AUF1} RNP complexes but show that only a subset of the RNA ligand must be AU-rich. Although a short AU-rich domain is required to nucleate p37^{AUF1} RNP assembly (Fig. 1, *cf.* binding to Rβ_{31} *versus* Rβ_{17}-ARE$_{xx}$- Rβ_{17} ligands), significant contributions to complex stability are made by contacts with 5′-flanking RNA, and even more if a purine residue is present immediately downstream of the ARE domain (Figs. 2 and 7*A*). Energetic contributions to RNP stability by nucleotides 5′ of the core ARE domain include significant sequence-independent components, as additions of Rβ sequence (Fig. 2) yielded improvements in p37^{AUF1} binding affinity comparable to those observed with similarly extended ARE sequences (12). Although base-independent stabilization of RNP complexes often involves ionic interactions between the protein and the RNA phosphodiester backbone, this is incon-

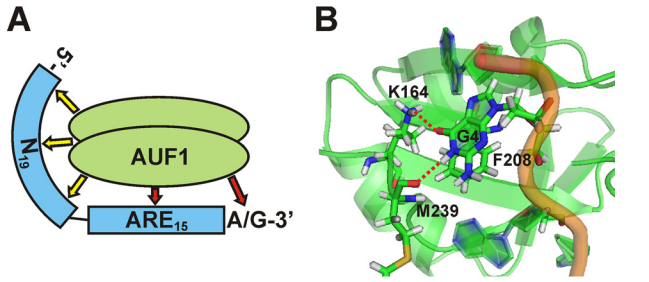

FIGURE 7. **RNA contacts required for high affinity p37^{AUF1} binding.** *A*, schematic showing RNA domains contributing to stability of p37^{AUF1} RNP complexes on minimal ARE substrates. *Red arrows* point to RNA sequences making base-specific contacts, whereas *yellow arrows* denote nonspecific contacts 5′- of the nucleating ARE sequence that are also required for AUF1-induced remodeling of local RNA structure. *B*, the structure of the AUF1 RRM2 domain bound to a telomeric DNA repeat fragment (PDB code 1X0F from Ref. 63) shows potential protein interactions with the first G nucleotide (*G4*). Implications for AUF1 binding to minimal ARE ligands are discussed under "Discussion."

sistent with the inability of 5′-Rβ sequences to alter the sensitivity of p37^{AUF1}-RNA binding equilibria to changes in ionic strength (Fig. 4 and Table 3). These data suggest that alternative interactions are formed between p37^{AUF1} and these upstream nucleotides, which could include contacts with ribose moieties similar to those described for HuR (62).

We were surprised to discover a strong enhancement to p37^{AUF1} binding by the presence of a 3′-purine. Using guanosine as a model, the enthalpic benefit conferred by this residue coupled with the increased entropic penalty associated with p37^{AUF1} binding suggests the formation of chemical contacts between this nucleotide and AUF1 (Table 3). Furthermore, the clear preference for a purine *versus* a pyrimidine base at this position indicates that such contacts likely involve direct base recognition. Further support for this model is given by the NMR structure of the C-terminal RRM of AUF1 bound to telomeric repeat d(TTAGGG) DNA, in which the RRM makes direct contacts with the central TAG sequence (63). In this structure the G nucleobase at position 4 is hydrogen-bonded to the carbonyl oxygen of Met-239 via N^1 and the ϵ-amino group of Lys-164 via O^6 while also forming a stacking interaction with Phe-208 (amino acid numbering follows p37^{AUF1} sequence) (Fig. 7*B*). An adenosine at this position would be similarly expected to stack well with Phe-208 and form the hydrogen bond between N^1 and the Met-239 carbonyl oxygen, although it would not form the second predicted hydrogen bond with Lys-164 because it lacks the O^6 acceptor. By contrast, pyrimidines would be unlikely to reach as deeply into the binding cleft to make the hydrogen bonds or stack with Phe-208. Also, a single purine 3′ of the U trinucleotide repeat of the core ARE was not sufficient to direct this enhancement of RNP stability (Fig. 2, *cf.* Fl-ARE$_{16}$ *versus* Fl-ARE$_{15}$-A), consistent with interactions observed between AUF1 RRM2 and each of the consecutive T, A, and G bases in the NMR structure (63). However, given that p37^{AUF1} can also bind with low nM affinity to extended ($\geq$34 nt) ARE domains that lack these additional 3′-purine residues (12), we suggest that the purine base is not necessary for association with all ARE-containing transcripts but could enhance binding on otherwise suboptimal targets. Furthermore, the presence of an additional purine 3′ of the core AU-rich domain may preferentially direct AUF1 to a specific binding register on an ARE, whose reiterative nature might otherwise present a quasi-homogeneous lattice of potential AUF1 binding sites.

His$_6$-p37^{AUF1} binding modified the conformation of the 35-nt Cy3-Rβ_{19}-ARE$_{15}$-G-Fl substrate by bringing the RNA 5′- and 3′-termini into closer proximity, an effect that was not observed with the Cy3-ARE$_{15}$-G-Fl RNA ligand (Fig. 5). Inclusion of the Rβ_{19} domain also correlated with the significantly increased negative value of $\Delta C^{\circ}_{P,obs}$ associated with p37^{AUF1} RNP formation (Table 2), suggesting that protein-induced alterations in RNA confirmation may contribute to the Rβ_{19}-dependent change in heat capacity. If so, it is possible that fewer nucleotides of sequence upstream of the ARE$_{15}$ core domain may be sufficient to induce these RNA conformational changes, as increased negative values of $\Delta C^{\circ}_{P,obs}$ were also observed for RNA substrates Rβ_8-ARE$_{15}$-G and Rβ_8-ARE$_{15}$ *versus* ARE$_{15}$-G upon binding to His$_6$-p37^{AUF1} (Table 2). Based on Equation 15, the average distance between the 5′- and 3′-termini of the Cy3-Rβ_{19}-ARE$_{15}$-G-Fl substrate is ~48 Å in the p37^{AUF1} RNP complex, in contrast to 60 Å between the ends of the unbound RNA ligand. These distances are similar to those observed for ARE$_{38}$-based RNA substrates (12, 33), suggesting that both extended ARE and chimeric Rβ-ARE ligands assume comparable conformations in AUF1 RNPs. Formation of such condensed RNA structures would likely involve protein contacts at or near both ends of the RNA ligand that bring its termini into close proximity and restrict RNA mobility. The additional protein-RNA contacts required by this model would also be consistent with increased enthalpic contributions to complex stability ($\Delta H^{\circ} < 0$) while decreasing system entropy ($\Delta S^{\circ} < 0$) (Table 2). Similar conformational rearrangements of bound single-stranded nucleic acid ligands have also been reported for the tandem RRM domain of hnRNP A1 and the RRM3+RRM4 domain of polypyrimidine tract-binding protein (PTB) (64, 65). For PTB in particular, association of individual RRMs with separate 6-nt polypyrimidine sequences permits the intervening nucleotides to be looped, potentially allowing distal sequence determinants to be co-localized in the RNP complex (65). However, telomeric DNA sequences binding to the tandem RRMs of hnRNP A1 make contacts with only 11 contiguous nucleotides (23), whereas a 27-nt RNA ligand (two 6-nt polypyrimidine sequences separated by a 15-nt spacer) is sufficient to bind the PTB RRM3+RRM4 domain with low nM affinity (65). By contrast, optimal binding of p37^{AUF1} requires at least 34 nt of RNA (Ref. 12 and this study). It is possible that the relative positioning of the two RRM domains in p37^{AUF1} require access to disparate RNA subdomains analogous to the PTB model, although involving greater spatial separation. However, the stepwise improvement in His$_6$-p37^{AUF1} affinity observed as a function of total RNA size (Fig. 2) suggests that RNA interactions involving AUF1 domains outside the RRMs or with RRM domains from both proteins in the dimeric AUF1 complex are more likely explanations on extended RNA substrates.

At present, >20 different ARE-binding proteins have been identified that confer diverse effects on the stability and translational efficiency of targeted mRNAs (2, 3). Given the variety of these factors expressed in cells, it is likely that many ARE-containing mRNA substrates are regulated by different proteins

through competitive and/or combinatorial mechanisms, a model supported by common mRNA substrates identified in ribonome-wide surveys of mRNAs targeted by distinct ARE-binding proteins (50, 66, 67). However, although each ARE-binding protein is recruited to AREs or similar sequences, biochemical analyses have indicated protein-dependent differences in ARE binding affinity, RNA sequence preferences, and sensitivity to local RNA structure (12, 21, 22, 53, 68). The current study provides a biochemical rationale for AUF1 binding to a broad range of ARE-like RNA targets beyond extended U-rich domains. Most notably, a 15–16-nt AU-rich sequence contained within a larger RNA context is sufficient to nucleate high affinity $p37^{AUF1}$ RNP complexes (Figs. 1 and 2) that can target substrate mRNAs for degradation in cells (Fig. 6). We predict that smaller ARE targets may focus *trans*-factor selectivity and minimize the potential for combinatorial binding mechanisms by limiting access to ARE sequence determinants beyond a single RNA-binding event. This model may explain the slower decay kinetics of the βG-RAR *versus* βG-ARE_{38} mRNAs in both shControl- and shAUF1-expressing HeLa cells (Table 4). Although $p37^{AUF1}$ bound both mRNAs in cells and significantly accelerated their decay kinetics, it is likely that some other cellular ARE binding factors were less efficiently recruited to the RAR reporter transcript and hence did not contribute to its turnover.

Finally, this study demonstrates that interactions between $p37^{AUF1}$ and RNA sequences 5′ of a nucleating ARE site mediate AUF1-induced changes in local RNA structure. Although the functional significance of this activity is currently unknown, we predict that these conformational changes may enhance or obstruct access for other RNA binding factors or microRNAs to nearby binding sites on mRNA targets. These factors could include members of a multisubunit *trans*-acting complex that may mediate AUF1-dependent effects on mRNA decay such as the heat shock proteins Hsp27 and Hsp/Hsc70, the translation initiation factor eIF4G, and poly(A)-binding protein (30, 69, 70). Most of these factors also possess RNA binding activity (30, 51, 71, 72), so local RNA remodeling by AUF1 could influence their recruitment by exposing adjacent sequence determinants. Alternatively, AUF1 binding may alter the accessibility of proximal RNA binding sites to other ARE-binding proteins or microRNAs. Future studies will determine which of these factors are impacted by AUF1-induced RNA remodeling and the functional significance of these RNA allosteric relationships.

Acknowledgments—We thank Aleksandra Wisniewska for assistance in assembling the AUF1 expression vectors and Drs. Gary Brewer and Bret Hassel for generously donating plasmids.

REFERENCES

1. Garneau, N. L., Wilusz, J., and Wilusz, C. J. (2007) The highways and byways of mRNA decay. *Nat. Rev. Mol. Cell Biol.* **8,** 113–126
2. Wu, X., and Brewer, G. (2012) The regulation of mRNA stability in mammalian cells: 2.0. *Gene* **500,** 10–21
3. Barreau, C., Paillard, L., and Osborne, H. B. (2005) AU-rich elements and associated factors. Are there unifying principles? *Nucleic Acids Res.* **33,** 7138–7150
4. Halees, A. S., El-Badrawi, R., and Khabar, K. S. (2008) ARED organism. Expansion of ARED reveals AU-rich element cluster variations between human and mouse. *Nucleic Acids Res.* **36,** D137–D140
5. Schoenberg, D. R., and Maquat, L. E. (2012) Regulation of cytoplasmic mRNA decay. *Nat. Rev. Genet.* **13,** 246–259
6. Khabar, K. S. (2010) Post-transcriptional control during chronic inflammation and cancer. A focus on AU-rich elements. *Cell. Mol. Life Sci.* **67,** 2937–2955
7. Wagner, B. J., DeMaria, C. T., Sun, Y., Wilson, G. M., and Brewer, G. (1998) Structure and genomic organization of the human AUF1 gene. Alternative pre-RNA splicing generates four protein isoforms. *Genomics* **48,** 195–202
8. Arao, Y., Kuriyama, R., Kayama, F., and Kato, S. (2000) A nuclear matrix-associated factor, SAF-B, interacts with specific isoforms of AUF1/hnRNP D. *Arch. Biochem. Biophys.* **380,** 228–236
9. Mili, S., Shu, H. J., Zhao, Y., and Piñol-Roma, S. (2001) Distinct RNP complexes of shuttling hnRNP proteins with pre-mRNA and mRNA. Candidate intermediates in formation and export of mRNA. *Mol. Cell. Biol.* **21,** 7307–7319
10. Zhang, W., Wagner, B. J., Ehrenman, K., Schaefer, A. W., DeMaria, C. T., Crater, D., DeHaven, K., Long, L., and Brewer, G. (1993) Purification, characterization, and cDNA cloning of an AU-rich element RNA-binding protein, AUF1. *Mol. Cell. Biol.* **13,** 7652–7665
11. Wilson, G. M., Lu, J., Sutphen, K., Sun, Y., Huynh, Y., and Brewer, G. (2003) Regulation of A+U-rich element-directed mRNA turnover involving reversible phosphorylation of AUF1. *J. Biol. Chem.* **278,** 33029–33038
12. Zucconi, B. E., Ballin, J. D., Brewer, B. Y., Ross, C. R., Huang, J., Toth, E. A., and Wilson, G. M. (2010) Alternatively expressed domains of AU-rich element RNA-binding protein 1 (AUF1) regulate RNA-binding affinity, RNA-induced protein oligomerization, and the local conformation of bound RNA ligands. *J. Biol. Chem.* **285,** 39127–39139
13. Lin, S., Wang, W., Wilson, G. M., Yang, X., Brewer, G., Holbrook, N. J., and Gorospe, M. (2000) Down-regulation of cyclin D1 expression by prostaglandin A_2 is mediated by enhanced cyclin D1 mRNA turnover. *Mol. Cell. Biol.* **20,** 7903–7913
14. Raineri, I., Wegmueller, D., Gross, B., Certa, U., and Moroni, C. (2004) Roles of AUF1 isoforms, HuR and BRF1 in ARE-dependent mRNA turnover studied by RNA interference. *Nucleic Acids Res.* **32,** 1279–1288
15. Sarkar, B., Xi, Q., He, C., and Schneider, R. J. (2003) Selective degradation of AU-rich mRNAs promoted by the p37 AUF1 protein isoform. *Mol. Cell. Biol.* **23,** 6685–6693
16. Chen, T.-M., Hsu, C.-H., Tsai, S.-J., and Sun, H. S. (2010) AUF1 p42 isoform selectively controls both steady-state and PGE_2-induced *FGF9* mRNA decay. *Nucleic Acids Res.* **38,** 8061–8071
17. Lund, N., Milev, M. P., Wong, R., Sanmuganantham, T., Woolaway, K., Chabot, B., Abou Elela, S., Mouland, A. J., and Cochrane, A. (2012) Differential effects of hnRNP D/AUF1 isoforms on HIV-1 gene expression. *Nucleic Acids Res.* **40,** 3663–3675
18. Wilson, G. M., Sun, Y., Lu, H., and Brewer, G. (1999) Assembly of AUF1 oligomers on U-rich RNA targets by sequential dimer association. *J. Biol. Chem.* **274,** 33374–33381
19. DeMaria, C. T., and Brewer, G. (1996) AUF1 binding affinity to A+U-rich elements correlates with rapid mRNA degradation. *J. Biol. Chem.* **271,** 12179–12184
20. Wilson, G. M., Sutphen, K., Moutafis, M., Sinha, S., and Brewer, G. (2001) Structural remodeling of an A+U-rich RNA element by cation or AUF1 binding. *J. Biol. Chem.* **276,** 38400–38409
21. Fialcowitz, E. J., Brewer, B. Y., Keenan, B. P., and Wilson, G. M. (2005) A hairpin-like structure within an AU-rich mRNA-destabilizing element regulates *trans*-factor binding selectivity and mRNA decay kinetics. *J. Biol. Chem.* **280,** 22406–22417
22. Fialcowitz-White, E. J., Brewer, B. Y., Ballin, J. D., Willis, C. D., Toth, E. A., and Wilson, G. M. (2007) Specific protein domains mediate cooperative assembly of HuR oligomers on AU-rich mRNA-destabilizing sequences. *J. Biol. Chem.* **282,** 20948–20959
23. Ding, J., Hayashi, M. K., Zhang, Y., Manche, L., Krainer, A. R., and Xu, R.-M. (1999) Crystal structure of the two-RRM domain of hnRNP A1 (UP1) complexed with single-stranded telomeric DNA. *Genes Dev.* **13,** 1102–1115

24. Bakheet, T., Williams, B. R., and Khabar, K. S. (2006) ARED 3.0. The large and diverse AU-rich transcriptome. *Nucleic Acids Res.* **34,** D111–D114
25. Mazan-Mamczarz, K., Kuwano, Y., Zhan, M., White, E. J., Martindale, J. L., Lal, A., and Gorospe, M. (2009) Identification of a signature motif in target mRNAs of RNA-binding protein AUF1. *Nucleic Acids Res.* **37,** 204–214
26. Wu, X., Chesoni, S., Rondeau, G., Tempesta, C., Patel, R., Charles, S., Daginawala, N., Zucconi, B. E., Kishor, A., Xu, G., Shi, Y., Li, M. L., Irizarry-Barreto, P., Welsh, J., Wilson, G. M., and Brewer, G. (2013) Combinatorial mRNA binding by AUF1 and Argonaute 2 controls decay of selected target mRNAs. *Nucleic Acids Res.* **41,** 2644–2658
27. He, C., and Schneider, R. (2006) 14-3-3σ is a p37 AUF1-binding protein that facilitates AUF1 transport and AU-rich mRNA decay. *EMBO J.* **25,** 3823–3831
28. Heyduk, T., Ma, Y., Tang, H., and Ebright, R. H. (1996) Fluorescence anisotropy. Rapid, quantitative assay for protein-DNA and protein-protein interaction. *Methods Enzymol.* **274,** 492–503
29. Wilson, G. M., Sutphen, K., Chuang Ky, and Brewer, G. (2001) Folding of A+U-rich RNA elements modulates AUF1 binding. Potential roles in regulation of mRNA turnover. *J. Biol. Chem.* **276,** 8695–8704
30. Sinsimer, K. S., Gratacós, F. M., Knapinska, A. M., Lu, J., Krause, C. D., Wierzbowski, A. V., Maher, L. R., Scrudato, S., Rivera, Y. M., Gupta, S., Turrin, D. K., De La Cruz, M. P., Pestka, S., and Brewer, G. (2008) Chaperone Hsp27, a novel subunit of AUF1 protein complexes, functions in AU-rich element-mediated mRNA decay. *Mol. Cell. Biol.* **28,** 5223–5237
31. Sarkar, S., Sinsimer, K. S., Foster, R. L., Brewer, G., and Pestka, S. (2008) AUF1 isoform-specific regulation of anti-inflammatory IL10 expression in monocytes. *J. Interferon Cytokine Res.* **28,** 679–691
32. Wilson, G. M., and Brewer, G. (1999) Identification and characterization of proteins binding A+U-rich elements. *Methods* **17,** 74–83
33. Wilson, G. M., Lu, J., Sutphen, K., Suarez, Y., Sinha, S., Brewer, B., Villanueva-Feliciano, E. C., Ysla, R. M., Charles, S., and Brewer, G. (2003) Phosphorylation of $p40^{AUF1}$ regulates binding to A+U-rich mRNA-destabilizing elements and protein-induced changes in ribonucleoprotein structure. *J. Biol. Chem.* **278,** 33039–33048
34. Weber, G. (1952) Polarization of the fluorescence of macromolecules 1. theory and experimental method. *Biochem. J.* **51,** 145–155
35. Wilson, G. M. (2005) in *Reviews in Fluorescence* (Geddes, C. D., and Lakowicz, J. R., eds) Vol. 2, pp. 223–243, Springer Science+Business Media, Inc., New York
36. Lundblad, J. R., Laurance, M., and Goodman, R. H. (1996) Fluorescence polarization analysis of protein-DNA and protein-protein interactions. *Mol. Endocrinol.* **10,** 607–612
37. Hall, K. B., and Kranz, J. K. (1995) Thermodynamics and mutations in RNA-protein interactions. *Methods Enzymol.* **259,** 261–281
38. Ha, J.-H., Spolar, R. S., and Record, M. T., Jr. (1989) Role of the hydrophobic effect in stability of site-specific protein-DNA complexes. *J. Mol. Biol.* **209,** 801–816
39. deHaseth, P. L., Lohman, T. M., and Record, M. T. Jr. (1977) Nonspecific interaction of lac repressor with DNA. An association reaction driven by counterion release. *Biochemistry* **16,** 4783–4790
40. Lohman, T. M., and Mascotti, D. P. (1992) Thermodynamics of ligand-nucleic acid interactions. *Methods Enzymol.* **212,** 400–424
41. Lohman, T. M., deHaseth, P. L., and Record, M. T. Jr. (1980) Pentalysine-deoxyribonucleic acid interactions. A model for the general effects of ion concentrations on the interactions of proteins with nucleic acids. *Biochemistry* **19,** 3522–3530
42. Record, M. T., Jr., Lohman, M. L., and deHaseth, P. (1976) Ion effects on ligand-nucleic acid interactions. *J. Mol. Biol.* **107,** 145–158
43. Lohman, T. M. (1986) Kinetics of protein-nucleic acid interactions. Use of salt effect to probe mechanisms of interaction. *CRC Crit. Rev. Biochem.* **19,** 191–245
44. Record, M. T. Jr., Woodbury, C. P., and Lohman, T. M. (1976) Na^+ effects on transitions of DNA and polynucleotides of variable linear charge density. *Biopolymers* **15,** 893–915
45. Record, M. T. Jr., Anderson, C. F., and Lohman, T. M. (1978) Thermodynamic analysis of ion effects on the binding and conformational equilibria of proteins and nucleic acids. The roles of ion association or release, screening, and ion effects on water activity. *Q. Rev. Biophys.* **11,** 103–178
46. Stickle, D. F., and Fried, M. G. (2007) Cation binding linked to a sequence-specific CAP-DNA complex. *Biophys. Chem.* **126,** 106–116
47. Fried, M. G., and Stickle, D. F. (1993) Ion-exchange reactions of proteins during DNA binding. *Eur. J. Biochem.* **218,** 469–475
48. Lakowicz, J. R. (1999) *Principles of Fluorescence Spectroscopy*, pp. 367–394, Kluwer Academic/Plenum, New York
49. Norman, D. G., Grainger, R. J., Uhrín, D., and Lilley, D. M. (2000) Location of cyanine-3 on double-stranded DNA. Importance for fluorescence resonance energy transfer studies. *Biochemistry* **39,** 6317–6324
50. Lal, A., Mazan-Mamczarz, K., Kawai, T., Yang, X., Martindale, J. L., and Gorospe, M. (2004) Concurrent *versus* individual binding of HuR and AUF1 to common labile target mRNAs. *EMBO J.* **23,** 3092–3102
51. Kishor, A., Tandukar, B., Ly, Y. V., Toth, E. A., Suarez, Y., Brewer, G., and Wilson, G. M. (2013) Hsp70 is a novel posttranscriptional regulator of gene expression that binds and stabilizes selected mRNAs containing AU-rich elements. *Mol. Cell. Biol.* **33,** 71–84
52. Ysla, R. M., Wilson, G. M., and Brewer, G. (2008) Assays of adenylate uridylate-rich element-mediated mRNA decay in cells. *Methods Enzymol.* **449,** 47–71
53. Brewer, B. Y., Malicka, J., Blackshear, P. J., and Wilson, G. M. (2004) RNA sequence elements required for high affinity binding by the zinc finger domain of tristetraprolin. Conformational changes coupled to the bipartite nature of AU-rich mRNA-destabilizing motifs. *J. Biol. Chem.* **279,** 27870–27877
54. Spolar, R. S., and Record, M. T. Jr. (1994) Coupling of local folding to site-specific binding of proteins to DNA. *Science* **263,** 777–784
55. Fisher, B. M., Ha, J.-H., and Raines, R. T. (1998) Coulombic forces in protein-RNA interactions. Binding and cleavage by ribonuclease A and variants at Lys-7, Arg-10, and Lys-66. *Biochemistry* **37,** 12121–12132
56. Draper, D. E. (1995) Protein-RNA recognition. *Annu. Rev. Biochem.* **64,** 593–620
57. Ballin, J. D., Prevas, J. P., Ross, C. R., Toth, E. A., Wilson, G. M., and Record, M. T., Jr. (2010) Contributions of the histidine side chain and the N-terminal α-amino group to the binding thermodynamics of oligopeptides to nucleic acids as a function of pH. *Biochemistry* **49,** 2018–2030
58. Baumann, C., Otridge, J., and Gollnick, P. (1996) Kinetic and thermodynamic analysis of the interaction between TRAP (*trp* RNA-binding attenuation protein) of *Bacillus subtilis* and *trp* leader RNA. *J. Biol. Chem.* **271,** 12269–12274
59. Katsamba, P. S., Myszka, D. G., and Laird-Offringa, I. A. (2001) Two functionally distinct steps mediate high affinity binding of U1A protein to U1 hairpin II RNA. *J. Biol. Chem.* **276,** 21476–21481
60. Martin, K. J., and Schleif, R. F. (1987) Equilibrium DNA-binding of AraC protein. Compensation for displaced ions. *J. Mol. Biol.* **195,** 741–744
61. White, E. J., Brewer, G., and Wilson, G. M. (2013) Post-transcriptional control of gene expression by AUF1. Mechanisms, physiological targets, and regulation. *Biochim. Biophys. Acta* **1829,** 680–688
62. Wang, H., Zeng, F., Liu, Q., Liu, H., Liu, Z., Niu, L., Teng, M., and Li, X. (2013) The structure of the ARE-binding domains of Hu antigen R (HuR) undergoes conformational changes during RNA binding. *Acta Crystallogr. D Biol. Crystallogr.* **69,** 373–380
63. Enokizono, Y., Konishi, Y., Nagata, K., Ouhashi, K., Uesugi, S., Ishikawa, F., and Katahira, M. (2005) Structure of hnRNP D complexed with single-stranded telomere DNA and unfolding of the quadruplex by heterogenous nuclear ribonucleoprotein D. *J. Biol. Chem.* **280,** 18862–18870
64. Barraud, P., and Allain, F. H. (2013) Solution structure of the two RNA recognition motifs of hnRNP A1 using segmental isotope labeling. How the relative orientation between RRMs influences the nucleic acid binding topology. *J. Biomol. NMR* **55,** 119–138
65. Lamichhane, R., Daubner, G. M., Thomas-Crusells, J., Auweter, S. D., Manatschal, C., Austin, K. S., Valniuk, O., Allain, F. H., and Rueda, D. (2010) RNA looping by PTB. Evidence using FRET and NMR spectroscopy for a role in splicing repression. *Proc. Natl. Acad. Sci. U.S.A.* **107,** 4105–4110
66. Raghavan, A., Robison, R. L., McNabb, J., Miller, C. R., Williams, D. A., and Bohjanen, P. R. (2001) HuA and tristetraprolin are induced following T cell activation and display distinct but overlapping RNA binding specificities. *J. Biol. Chem.* **276,** 47958–47965

67. Winzen, R., Thakur, B. K., Dittrich-Breiholz, O., Shah, M., Redich, N., Dhamija, S., Kracht, M., and Holtmann, H. (2007) Functional analysis of KSRP interaction with the AU-rich element of interleukin-8 and identification of inflammatory mRNA targets. *Mol. Cell. Biol.* **27,** 8388–8400
68. Kim, H. S., Wilce, M. C., Yoga, Y. M., Pendini, N. R., Gunzburg, M. J., Cowieson, N. P., Wilson, G. M., Williams, B. R., Gorospe, M., and Wilce, J. A. (2011) Different modes of interaction by TIAR and HuR with target RNA and DNA. *Nucleic Acids Res.* **39,** 1117–1130
69. Laroia, G., Cuesta, R., Brewer, G., and Schneider, R. J. (1999) Control of mRNA decay by heat shock-ubiquitin-proteasome pathway. *Science* **284,** 499–502
70. Lu, J. Y., Bergman, N., Sadri, N., and Schneider, R. J. (2006) Assembly of AUF1 with eIF4G-poly(A) binding protein complex suggests a translation function in AU-rich mRNA decay. *RNA* **12,** 883–893
71. Matsui, H., Asou, H., and Inaba, T. (2007) Cytokines direct the regulation of *Bim* mRNA stability by heat-shock cognate protein 70. *Mol. Cell* **25,** 99–112
72. Görlach, M., Burd, C. G., and Dreyfuss, G. (1994) The mRNA poly(A)-binding protein. Localization, abundance, and RNA-binding specificity. *Exp. Cell Res.* **211,** 400–407